UNIVERSITY OF THE
WITWATERSRAND,
JOHANNESBURG

Synthesizing Carbon and Ceria Supported Pd Electrocatalysts for Alcohol Fuel Cell Systems

MSc Research Dissertation Submission

Prepared by

Suhail Ahmed Musa

(742699)

Submitted to

School of Chemical and Metallurgical Engineering, Faculty of Engineering and the Built Environment, University of the Witwatersrand, Johannesburg, South Africa

Supervisors: Prof Kenneth Ozoemena and Prof Iakovos Sigalas

April, 2020

Acknowledgements

The research and knowledge outcomes achieved through this project could not have been done alone.

Therefore, I would like to thank Prof Iakovos Sigalas for introducing me to the post graduate world. I would also like to thank Prof Kenneth Ozoemena who, more than anyone else, deserves the credit for the position I am in today. Your knowledge, guidance, critical thinking, and most importantly character; provided a source of light when the work seemed overwhelming.

Most importantly, I would like to thank my parents for always supporting me through every decision I have made in my life. Knowing that you are there to catch me when I fall is the reason I can leap so often. Finally, I wish to thank my older brother, Ryaz. A role model ever since I could remember and a man whose advice I readily take – be it academic or life in general.

Thank you all for the love and support.

Glossary

AGFCS = Alcohol Gas Fuel Cell Sensor

BAC = Blood Alcohol Concentration

BET = Brunauer Emmett Teller

BrAC =Breath Alcohol Concentration

CB = Carbon Black

CV = Cyclic Voltammetry

ECSA = Electrochemically Active Surface Area

EDS = Energy Dispersive Spectroscopy

EIS = Electrochemical Impedence Spectroscopy

IRS = Infrared Spectroscopy

LSV = Linear Sweep Voltammetry

OLC = Onion Like Carbon

PEMFC = Proton Exchange Membrane Fuel Cell

REDOX = Oxidation-Reduction

RSA = Raman Spectroscopy Analyses

SEM = Scanning Electron Microscope

TGA = Thermogravimetric Analyses

XRD = X-ray Diffraction

List of Figures

Table of Contents

1. Introduction

A fuel cell is based on a rather simple design (hence the popularity of use in various industries) and is made up of multiple components tightly pressed together to form the unit – commonly referred to as the Membrane Electrode Assembly or MEA. The key components that a fuel cell is made up off includes but is not limited to: gas diffusion electrodes (GDEs) – alternatively referred to as the anode and cathode chambers; electrolyte – ion carrier/transporter from one electrode to the other (solid or liquid); electrically conducting wire; electro-catalyst – catalyst used to speed up one or more half reactions; the gasses used – although not technically a component of the fuel cell, they are required in order to function. The focus of this research lies with the electro-catalyst. The basic principle of a fuel cell is converting chemical energy into electricity. This is accomplished by a REDOX reaction – An electron (e^-) is extracted from the alcohol (fuel – typically hydrogen based) and passed through an external circuit, generating a minor current, and flows to the other GDE where it combines with oxygen. The site at which both extraction and attachment of the electron occurs, is the catalytic surface – usually platinum. The by-product that is formed in this process is water – which made up of the oxygen present in the cathode bonding with the H^+ ions passing through the electrolyte and e^- through the external circuit [1]. This is explained in greater detail in sections 1 and 2.

Expendable/primary cells are those cells that have one life and after they are depleted, they are discarded. Secondary cells on the other hand have life cycles – that is, they can be used until depletion then recharged or refuelled with reactants so that they may serve their purpose again (thus being cycled multiple times).

Electrochemical cells (such as torch batteries and fuel cells) are devices that convert chemical-potential energy into electricity. Due to the electrical nature inherently existing in chemical bonds, the conversion from chemical energy into electrical energy is a straight forward path. These cells bypass the heat degradation step existing in most mechanical energy conversion tools, they are not limited by the Carnot efficiency and the amount of reactants used can be easily and accurately measured.[11]

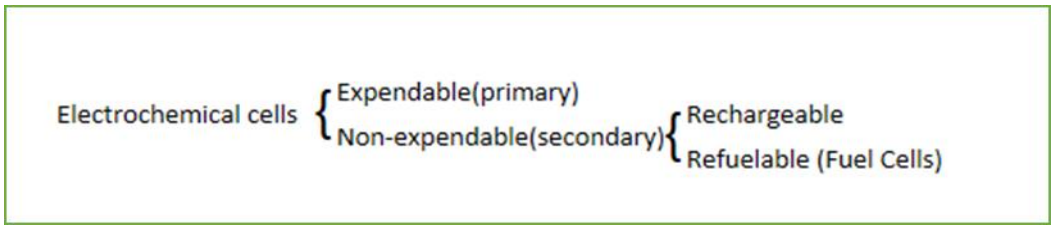

2. Literature Review

2.1. Basics of a Fuel Cell

2.1.1. Overview (Components and Design)

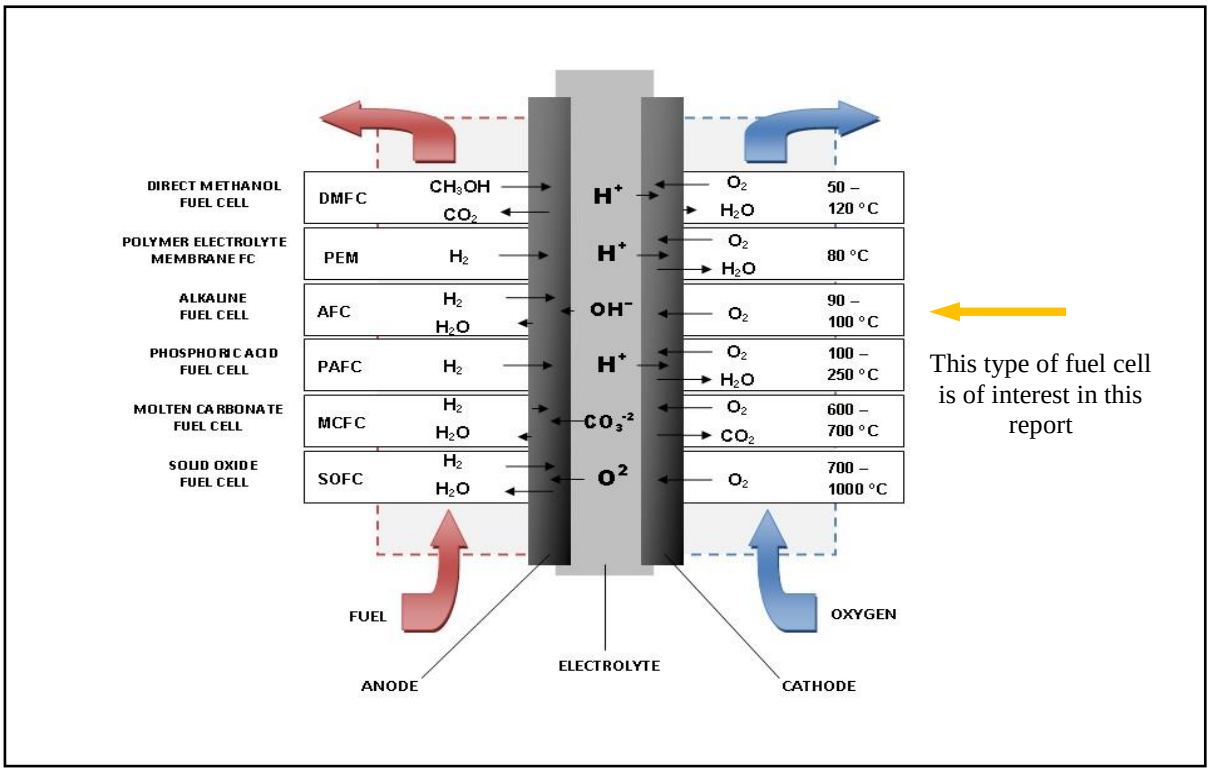

Figure 1: Different Transfer ions based on type of cell designed [11]

It has been observed that the underlying technology and components of the breathalyser have not been updated for decades and the current generation of units are still based on 1970s technology.[2] This design involves a high use of platinum as the electro-catalyst, a very expensive metal. Due to many important advancements in technology since then, it is believed that a far cheaper alcohol gas sensor can be designed, minimizing the platinum concentration or replacing it completely and thus making a more feasible sensor without inhibiting sensitivity, reliability, and durability.[3] This will allow for them to be readily and/or easily available in low/middle income countries that make up for 90% of the world's road accidents [4,5]. Palladium has shown to be a viable electro-catalyst. According to the study performed by Holton and Stevenson [6], palladium in its pure form was observed to only be marginally inferior as a bonding agent to oxygen than platinum. It was also observed that bi-metallic compounds could potentially be suitable electro-catalysts if the core metal itself was viable. Thus, it is proposed that a compound containing palladium as its core, and possibly supported

by ceramics or carbon nanofibers, could theoretically replace platinum as the leading electro-catalyst. This would drastically reduce both the manufacturing cost as well as the maintenance cost of the Alcohol Gas Fuel Cell Sensor (AGFCS) unit.

Although many other forms of alcohol detection such as gas chromatography, infrared, and semi-conductor [7,8,9] techniques are commercially available, breath ethanol detection is usually performed by fuel cell sensors owing to their linearity, accuracy, sensitivity, size, rapid response time, and cost. [10]

Several different kinds of Fuel cells exist as shown in Figure 1.There are many ways to categorize these devices, but the simplest way is looking at the reactant fuel and/or the electrolyte used [11]. Each type of fuel cell has their own advantages and disadvantages and are chosen based on the need and working conditions of the user. The alkaline fuel cell is best suited for the objectives this research is set out to achieve – due to the alcohol reactant and temperature range.

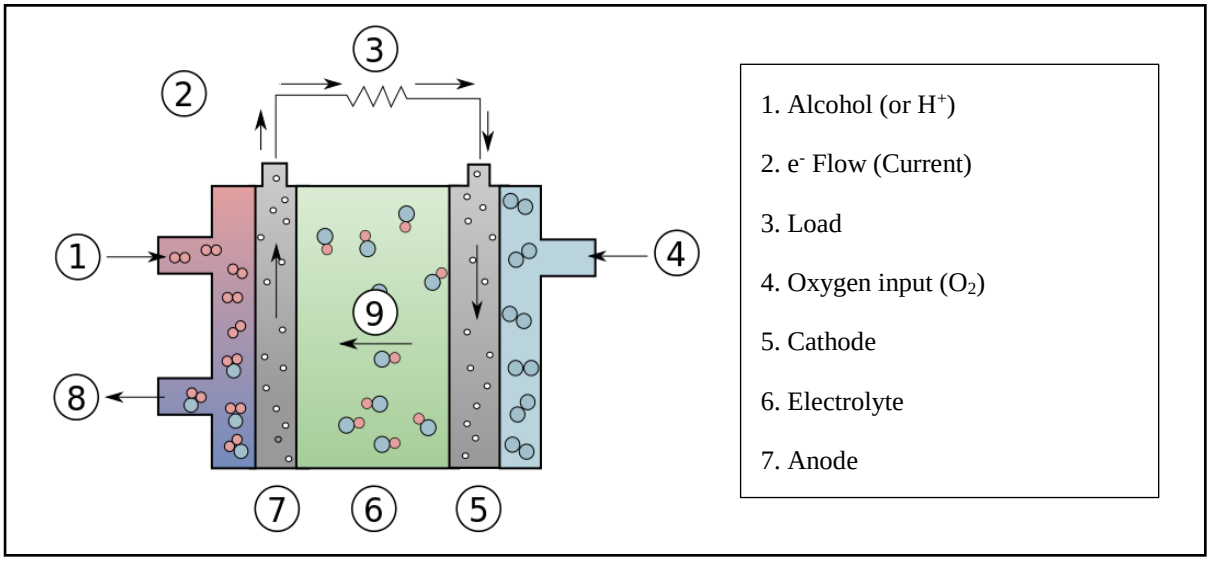

Figure 2: Alkaline Fuel Cell - OH transported through electrolyte [27]

An example of the mechanism and theory behind the alkaline fuel cell is shown in Figure 2 above. Since the by-product is water, fuel cells prove to be a great source of energy generation and chemical sensors. The electrocatalyst studied in this research will reside on the anode while the cathodic electrocatalyst will be comprised of some derivative of iron and cobalt (Future work).

The underlying purpose of all fuel cells is to generate a current. The current density (the amount of electric current flowing per unit cross-sectional area of a material) is determined by the concentration and/or amount of reactants that react. The faster the reaction rates of both AOR and ORR, the greater the expected current density[11]. For industrial based fuel cells, a high current density (relative to the amount of material in the electrode) is sought after. This is because the primary purpose of industrial fuel cells is current generation. The aim is to generate current from chemical energy (label 3 in Figure 2).

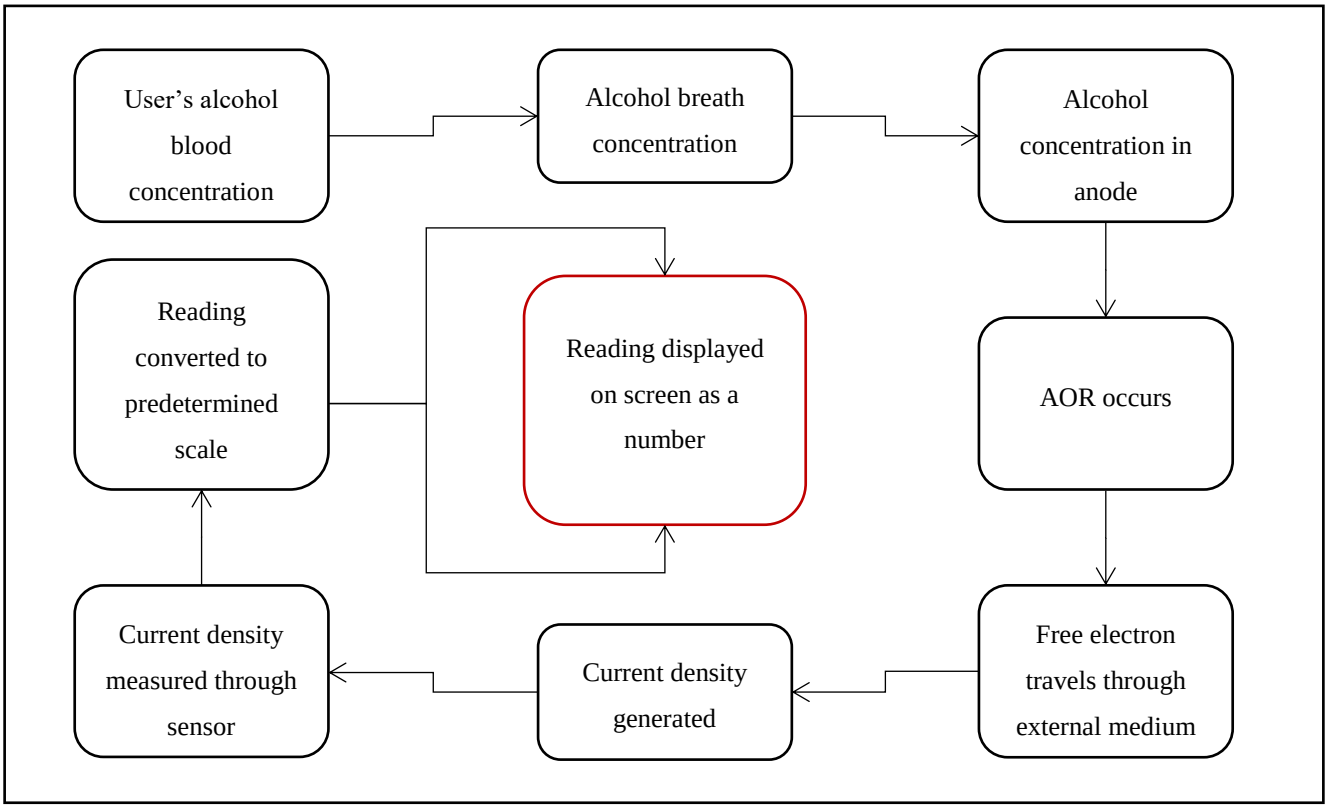

Figure 3: Current Generation and Readings

In this research, although current generation is a necessary step, the aim is not to achieve a high charge density nor utilize this electrical energy for other uses but rather to simply measure the electricity generated as it is an indication of the concentration of alcohol. Here sensitivity plays a rather important role as opposed to raw power output. The current and charge densities would be plotted against the present breath alcohol concentrations (BrAC). The slope produced by these curves would indicate the catalyst's sensitivity and combined with the regression of the curves, the linearity could be calculated. Once the required formulae are derived, they can be

used to translate the current generated when used by the subject into the appropriate BrAC. This concentration of alcohol in the breath can then be used to determine the amount of alcohol present in the user's blood and thus one can determine if the user is above the alcohol limit or not. A simplified schematic diagram of the process is shown in Figure 3. The displayed number is related to the user's alcohol breath, and therefore blood, concentration. Based on Henry's law, the ratio of exhaled alcohol to blood alcohol is 2100:1 [15]. More simply, if *x* amount of alcohol exists in 2100 millilitres of exhaled air, then *x* amount of alcohol exists in 1 millilitre of blood.

2.1.2. Alkaline vs Acidic Electrolyte

Fuel cells are sometimes categorized not by the reactants but rather by the electrolyte used. The electrolyte is responsible for transporting the necessary ion from one electrode to the other. This is a purely concentration-based diffusion step. Should the electrolyte fail to transport the ion (H^+ in most cases but could potentially be OH^- in an alkaline fuel cell or even O_2), the whole process would be at a standstill and reactants would build up in their respective electrodes. This selective transportation of molecules thus has a significant impact on the functionality of the cell and links to reaction rates, current density generated, and peak current generated. [1]

Electrolytes have primarily, in the past, been liquids. However, due to advancements in technology as well as the need to have mobile fuel cells, solid electrolytes are now the preferred medium. Nafion can help attach the catalyst layer to the membrane, and it also helps increase the ionic conductivity of the catalyst layer [1]. According to H_2/air PEMFC testing, Nafion 112 (one of the many industrially used forms of Nafion) has reached a maximum lifetime of just over 10,000 hours - a significantly acceptable number of cycles. [12]

The research focuses on the electrocatalyst involved in the PEMFC production and would thus produce results that are comparable to other catalysts, not other electrolytes. However, considering that multiple researchers also used a version of Nafion as their electrolyte. Nafion is likely the most viable material for comparative reasons in order for this research to minimize variations. [1, 5, 13]

Table 1: Acidic vs Alkaline Electrolytes

Acid Electrolyte	
Pros	**Cons**
Doesn't require very pure input gasses	Higher susceptibility to corrosion
Broad input fuel choices	Higher manufacturing costs
High tolerance for CO and CO_2 - more tolerant to impurities as compared to both solid oxide and alkaline FCs	Aggressive electrolyte – requires frequent maintenance
	Low power density
	Poor ionic conductor at low temperature
	Ni is not stable in this environment due to leaching
Alkaline Electrolyte	
Pros	**Cons**
Higher number of potential alternate catalysts	Requires a CO2 free environment to avoid poisoning – carbonates
Higher current densities / lower voltage drop at room temperature	Evolution of insoluble salts that could potentially block pores
Lower manufacturing costs	Require extremely pure into gasses – easy but expensive
Over 15000 hours of operating time	
Circulates oxygen more efficiently	
Easily removable waste products	
Highly cost effective	

2.1.3. Reaction Kinetics

According to Breeze *et al* (2009) [11], two half (redox) reactions occur in two separate regions of the fuel cell. The cell is primarily comprised of two separate chambers called electrodes – The anode and the cathode. In each of these chambers, a "half-reaction" occurs, i.e. the products of one and reactants of the other are intermediates and both reactions combined produce a stable overall reaction.

2.1.3.1. Anode Half Reactions

A reactive fuel (usually hydrogen gas or some alcohol) enters the anode. At the anode, AOR occurs. The basic pure hydrogen-based reaction occurring the anode indicated by Zhang in Equation 1 can be adapted to fit primary alcohols as shown in Equation 2[1]. This initial reaction converts the primary alcohol into an aldehyde, however this is not necessarily the end, the recently formed aldehyde can once again be oxidised into a carboxylic acid: this is dependent on the strength of the oxidising agent. If this occurs, the reaction process would proceed as shown in Equation 3.

Equation 1: Hydrogen half reaction

$$H_2 \rightarrow 2H^+ + 2e^- \ (acidic\ media)$$

$$H_2 + 2OH^- \rightarrow 2H_2O + 2e^- \ (alkaline\ media)$$

Equation 2: AOR part 1

$$R - CH_2 - OH \rightarrow R - CHO + 2H^+ + 2e^-$$

Equation 3: AOR part 2

$$R - CHO + H_2O \rightarrow R - COOH + 2H^+ + 2e^-$$

The overall AOR can thus be summarised as below if the alcohol is sufficiently oxidised

Equation 4: Complete AOR of primary alcohol

$$R - CH_2 - OH + H_2O \rightarrow R - COOH + 4H^+ + 4e^-$$

It should be noted that for the example above, water was assumed to be present in the fuel cell as the human breathe would contain moisture and can be modelled as saturated air - 100% Relative Humidity (RH) - at 32ºC as stated by Wilamed [13]. The water found here should not be confused with the water exiting the fuel cell at the cathode side, which is a by-product of the ORR.

2.1.3.2. Cathode Half Reactions

Air (assuming 21 volume % oxygen) or pure oxygen gas is fed into the cathode. At the Cathode, ORR occurs. Oxygen is broken down into individual oxygen atoms and adheres to the catalyst surface. The flowing hydrogen and electron then merge with these surface oxygen atoms/ions to form a hydroxide and then pure water - a safe by-product. The mechanism of these reactions are depicted by Varun Vij *et al* [14]

Equation 5: ORR

$$O_2 + 2H_2O + 4e^- \rightarrow 4OH^- \ (4\ electron\ process)$$

$$O_2 + H_2O + 2e^- \rightarrow OH^- + HO_2^- \ (2\ electron\ process - 1/2)$$

$$HO_2^- + H_2O + 2e^- \rightarrow 3OH^- \ (2\ electron\ process - 2/2)$$

The ORR could potentially experience minor complications. This is due to high-energy reaction kinetics / pathways and the relatively strong O-O bond in pure oxygen, not all the O_2 molecules break on the catalyst surface. This could result in a small concentration of H2O2 forming in the cathodic chamber or electrode. This is a highly corrosive compound and fortunately has a much smaller selectivity (the probability of a reaction to form the compound of interest against all possible products). The better the catalyst, the higher the selectivity of H2O [6]. A basic diagram can illustrate the possible alternate pathways oxygen gas may react through and is shown in Figure 4 below.

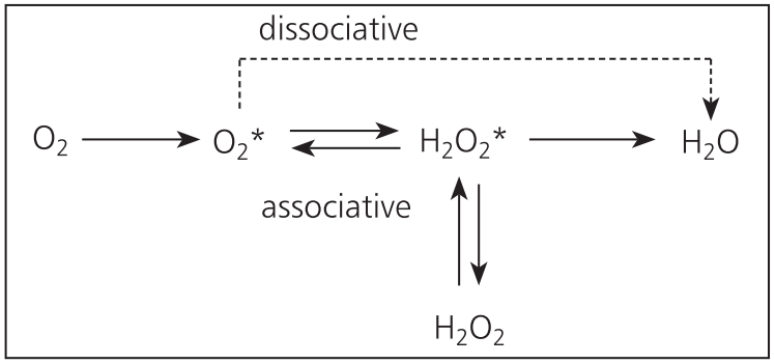

Figure 4: Alternate pathway for ORR [6]

Although ruthenium (Ru) and iridium (Ir) are the most efficient catalysts for oxygen evolution (refer to Figure 7), platinum (Pt) is regarded as the best catalyst for both hydrogen evolution as well as oxygen reduction. [14]. Even though Pt is the best for ORR, it is still not at a significantly remarkable level currently. Efforts should be made to enhance the ORR process significantly in the future.

2.1.4. Mass Transfer

A critical aspect in the efficiency and overall functioning of a fuel is the mass transfer (MT) stage. Mass transfer is achieved in multiple forms and include; Diffusion (region A) and Convection (Region B). The basic principal behind this is like that of heat transfer in the sense that materials (compounds) will move from a high state of energy (indicated by a large concentration since molecular interactions are more significant) to a low state. This is commonly referred to as the concentration gradient. Thus, the two state conditions effecting MT is the concentration of the bulk material and concentration at the surface of the electrode where the reaction occurs. It is also affected by temperature and pressure gradients but that is less impactful and can be assumed negligible for our research. The formula depicting MT is known as Fick's Law and is as follows;

$$J_i = -D_{ij} \cdot \nabla C_i$$

Where;

J_i = Mole flux (kg.mol/m^2.s)

D_{ij}= Diffusion coefficient (for two species)

$\cdot\nabla C_i$ = concentration gradient (kg.mol/m^3)

For multi-component diffusion systems (once again neglecting the pressure and temperature contributions), the Stephan-Maxwell equation can be used and is depicted as;

$$J_i = -C_i \cdot \sum_{j=1}^{n-1} D_{ij} \cdot \nabla x_j$$

Where;

J_i = Mole flux (kg.mol/m^2.s)

C_i = Concentration (kg.mol/m^3)

D_{ij}= Diffusion coefficient (for two species)

X = Mole fractions (unitless)

Convective MT would take place as a bulk flow is initiated – in this case, the channel from the anode and cathode chambers (see Figure 5 below), dragging species regardless of the concentration differences.

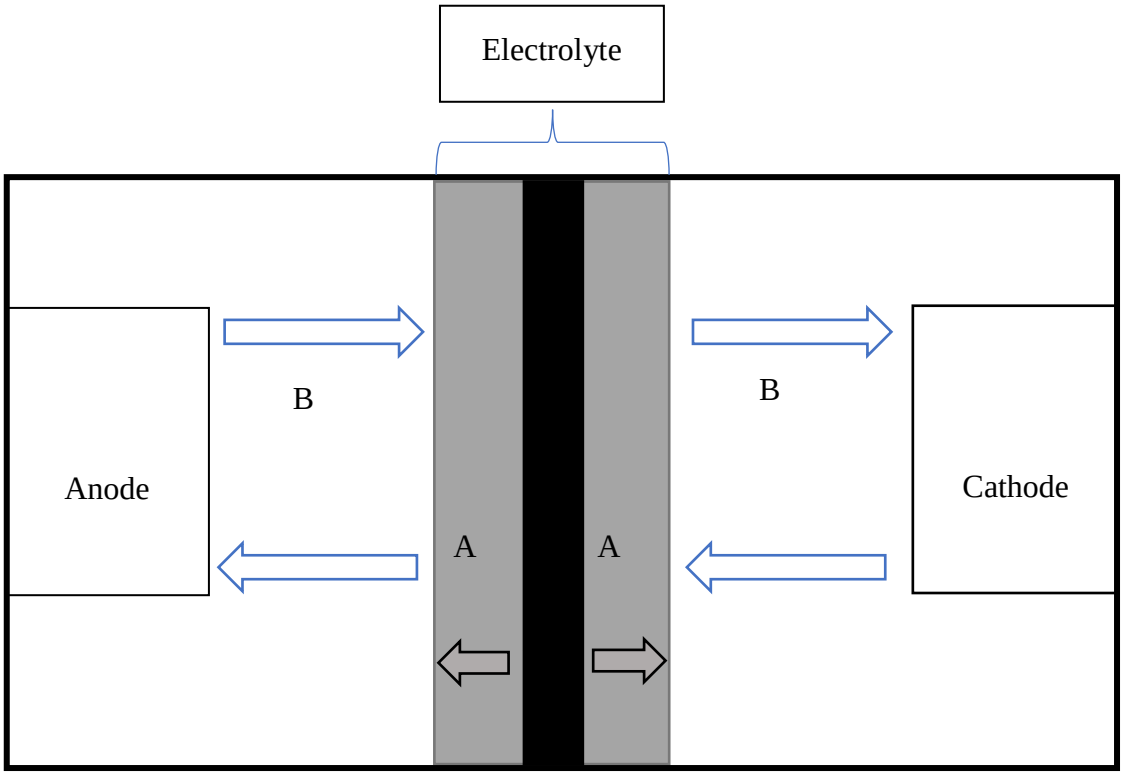

Figure 5: Mass Transfer Zones in a Fuel Cell

2.1.5. Fuel Cell Efficiency

Fuel Cell efficiency, just like any other is based off the ratio between the useful energy output against the energy input. Note that the actual efficiency of the system will either be equal to or lower than the theoretical efficiency calculated. For the fuel cell in general (and for this research as an alcohol gas sensing micro fuel cell), the useful output energy is the electrical energy produced in the external circuit explained above. The energy input is based of the chemical potential energy of the reactants – enthalpy of hydrogen gas. We can simplify the calculations by assuming that all the Gibbs-free energy can be converted into electrical energy without any waste. Since both the enthalpy and Gibbs-free energy are known, the maximum theoretical efficiency of a fuel cell at STP is [1];

$$\theta = \frac{\Delta G_f^o}{\Delta H^o} = \frac{237.1kJ/mol}{286kJ/mol} = 83\%$$

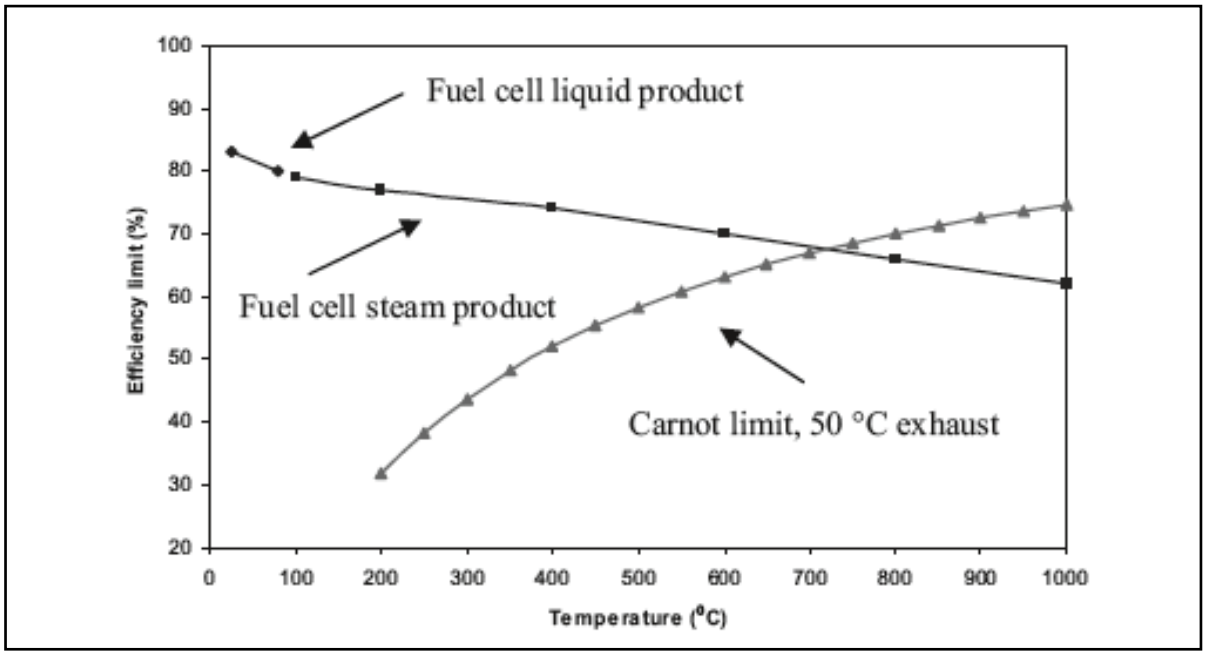

Figure 6: FC Efficiency as a Function of Operating Temperature [1]

The Gibbs-free potential and enthalpy potential can be obtained by dividing the respective term by the product of n.F. This yields values of 1.23V and 1.48V for the theoretical cell potential and hydrogen's Higher Heating Value (HHV) – aka thermoneutral potential respectively [1]. PEMFC plotted the efficiency of a FC against temperature (based on HHV) and is shown below. At higher operating temperatures for the FC, the efficiency is lower and could be attributed to wasted energy going into the formation of gaseous products for one. This provides justification to attempt operating at lower temperatures.

The equation can be specified to any FC by inputting the measured cell potential (V_{cell})

$$\theta = \frac{V_{cell}}{1.48} \cdot 100\% \ (If\ using\ HHV)$$

OR

$$\theta = \frac{V_{cell}}{1.23} \cdot 100\% \ (If\ using\ LHV)$$

However, considering that 100% conversion of the inputted fuel is not realistically achieved, the conversion factor must be considered to accurately determine the efficiency. Thus, the final equation is as follows;

$$\theta = \mu_f \cdot \frac{V_{cell}}{1.48} \cdot 100\% \ (If\ using\ HHV)$$

Where;

$$\mu_f = \frac{mass\ of\ fuel\ reacted}{mass\ of\ fuel\ inputted}$$

2.2. World's Leading Catalysts

2.2.1. Platinum

The catalyst primarily has two functions to perform without any change to itself (i.e. no leaching or degradation of any kind):

1) The catalyst adsorbs the elements that need undergo oxidation and/or reduction and hold them for a short period of time.
2) Once the molecules/elements react, the catalyst releases the product back into the Gas Diffusion Electrode (GDE).

Platinum has the best fit to both these functions. Platinum is a transition element that could easily form bonds with the hydrogen and oxygen molecules present in the GDE. However, some materials such as titanium and iridium form even more stable bonds yet are not considered. This is due to the second function of the catalyst, energy is needed to break up the bonds between catalyst and the given species – a bond too strong would require too much energy to break and would thus result in an accumulation of oxygen and/or hydrogen on the respective electro-catalyst [6]. Plots (known as volcano diagrams) obtained from Holton and Stevenson (2013) can be seen in Figures 7 and 8 [6]. A simple explanation is that the top of the peak is the best catalyst, those elements on the left bond too weakly (does not satisfy condition one above) while those on the right bond too strongly (does not satisfy condition two above). Conversely, bonds too weak would not be able to maintain the catalyst-hydrogen/oxygen bond and thus the reaction would proceed very slowly or not at all.

2.2.2. The Need for Alternatives

The electrochemical-based fuel cell sensor was introduced in the 1970s [15, 16]. According to Modjtahedi *et al.*[3], the current generation of breathalysers commercially used today is still based on the 1970s technology. Although this technology is acceptable to measure the gas concentration of an individual in terms of sensitivity, the manufacturing costs incurred during the production of these units are very high with Pt accounting for nearly 40% of the total production cost. With the advancements in technology made over nearly half a century since

then, the various components that make up a fuel cell are being re-examined to design a more feasible option – note that these advancements will also aid in sensitivity, durability and many other factors that will be discussed in further detail below.

As a result, the electro-catalyst (made of nearly 100% platinum) is currently under much scrutiny. Platinum is a costly material driving up manufacturing costs and is significantly poisoned on its surface by strongly adsorbed organic material – the reactant. This results in rapid degradation of the platinum catalyst and in turn requires regular replacement further adding to the costs [16].

2.3. Alternate Catalysts

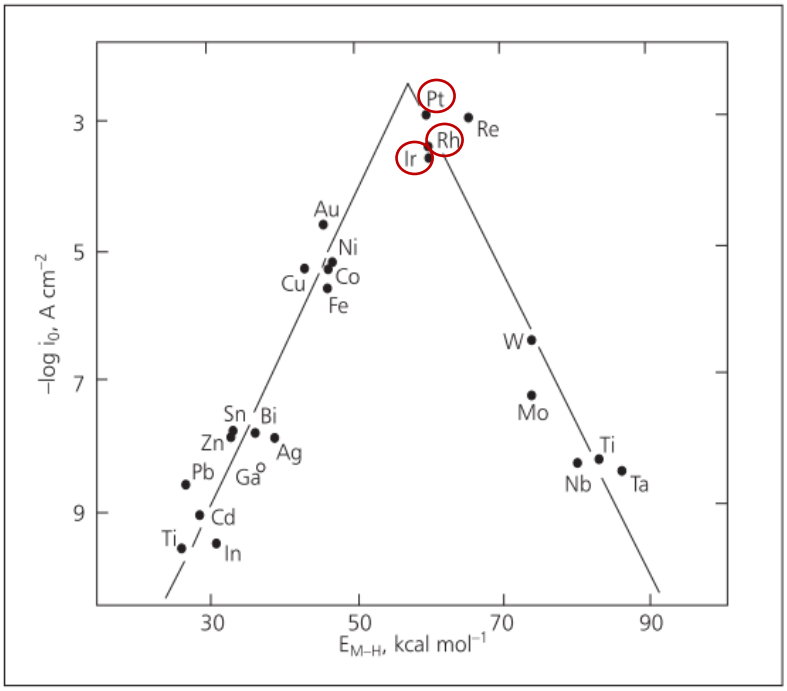

Figure 7: The log of exchange current densities for cathodic hydrogen evolution vs the adsorption strength of the metal-hydrogen bond during the reaction [6]

There are various factors that go into consideration when a system requires the “best catalyst”. The needs of the system need to be weighed. What is more important? Cheap production cost or raw performance? Sensitivity of the readings or durability of the device? In this sense, talking about an optimum catalyst is more apt than mentioning the best catalyst. Even though platinum reigns superior in most regard, there are other catalysts well worth being studied as possible replacements. The 2 major categories being production cost and durability. Looking

at Figure 7, it can be seen that 3 other elements reside near platinum. Another group involving nickel, cobalt, and iron depict slightly lower current densities for hydrogen evolution at a significantly lower adsorption energy of the metal-hydrogen bond.

2.3.1. Palladium (Pd)

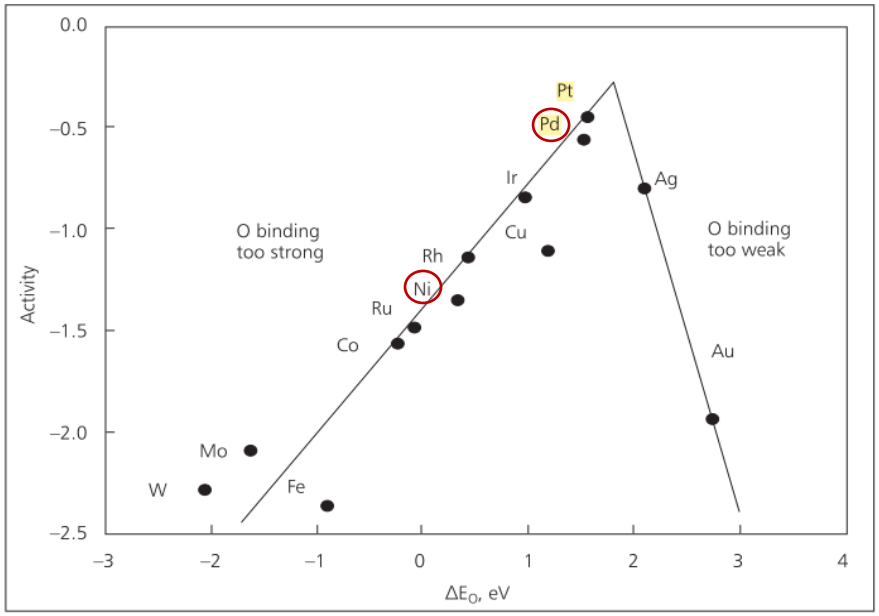

Figure 8: Oxygen binding energy against possible core catalysts [6]

Research for an alternative electrocatalyst is already underway. Many academics have performed individual AOR and ORR on multiple pure elements and the results from Holton and Stevenson[6] are displayed in Figures 7 and 8 respectively. The closer the element is to the peak, the greater its suitability to be an electro-catalyst. It is worth mentioning that elements to the left of the peak bond too weakly and elements on the right bond too strongly. Based on the grouping of Platinum Group Metals (PGMs) near the peak on Figure 8 and Palladium far exceeding the potential of the other elements. Palladium – a PGM – has been chosen as the core metal electro-catalyst for this project. It has similar electrochemical and physical properties as platinum but is denser and much more affordable. Palladium can prevalently oxidize most alcohols to their corresponding carboxylic acid – the exception to this is methanol which proceeds through intermediary of formate ($CHOO^-$) or carbon monoxide (CO). [17]

The Volcano diagram in Figure 8 shows Palladium as a great alternative as previously mentioned. However due to Nickel's incredible conductivity and ease of synchronisation as an alloy, it has seen countless studies as a filler catalyst. It also boasts great results on the volcano

plots, but previous studies suggest that merely alloying the metals near the top is not sufficient, as nickel has already proven to compete with copper and silver as platinum's core-shell.

2.3.2. Nickel (Ni)

With regards to water-splitting, a catalyst that would perform hydrogen evolution and oxygen evolution in the same electrolyte is desired. This would result in a simpler system design, improved practical applications, and lower cost. Ni is by far the most efficient bifunctional element used to catalyse this reaction in basic media[18, 19]. So far multiple Ni-based catalyst have already been developed. The downfall of these catalysts resides in the fact that they are not very stable and/or durable. Merging these catalysts in order to eliminate these shortcomings produce new challenges such as lower electrical conductivity and thus water splitting catalysts remain a huge challenge to this day.[20]

Varun *et al* concluded that Ni-based electrocatalysts have been extensively studied in the past and introducing other transition metals as an alloy has been established as the most promising approach in enhancing the number of active sites for the desired reactions. However, despite very high catalytic efficiencies and thermal stabilities of these alloys, the stability under highly concentrated electrolyte media proves to be a setback – This is something that needs to be resolved by enhancing our support material. Many scientists propose to replace Pt with Ni due to similar chemical properties, identical group number on the periodic table of elements, and the abundance of Ni found on earth which results in a significantly lower cost [19]

According to Bianchini *et al*, it is understood that Ni is oxophilic and has the capacity to facilitate OH^- adsorption at lower potentials and thus aids the oxidative desorption of the intermediate products which enhances the catalytic ability and stability of the Pd catalysts [17].

2.4. Support Materials

2.4.1. Carbon Black

Previous reports have studied the (intrinsic) electronic interaction between the catalyst and the carbon support to determine the potential influence on methanol [21, 22]. The binding energies of the 4*f* orbital for platinum and palladium were found to be higher for smaller sparticle sizes - in the case of Pt it was ~71.6eV for clusters and particles and ~71.1eV for the bulk catalyst.

The presence of carbon weakens the 4*f* electron binding making it more inclined to interact with and/or adsorb organic compounds. Heating the Pt/C catalyst also increased the 4*f* binding energy from 71.3eV to 72.2eV (673K for 4 hours). This is a result of the metal catalyst donating an e^- to the carbon support, lowering the overall activity of the system. Compared to the usual carbon black electrocatalysts, the nanotube-supported Pt catalyst resulted in up to 140% improvement in efficiency for a proton exchange membrane fuel cell (PEMFC) [23]. It had also been shown that the performance of a carbon nanotubes (CNT)-based MEA is superior to that of conventional Pt/C MEA [24]. Thus other derivatives of carbon should be tested. Although a high surface area would prove useful on many fronts, electrochemical stability is often sacrificed for this cause [14]. Thus, a balanced surface area would be viable for both a stable yet conductive catalyst support.

2.4.2. Onion-Like Carbon

Carbon onions or Onion-like carbons (OLCs) are quasi-spherical nanoparticles ranging from 5-10nm. They consist of concentric graphite shells which enclose fullerene-like carbons. Due to their highly symmetrical nature, they host different properties compared to more commonly known carbon derivatives such as nano-diamond, carbon tubes, vulcan carbon, and nanotubes amongst others. They have a range of applications from magnetic recording systems to aiding in the attachment of desirable functional groups. Their lack of interest in commercial research was due to the inability to mass produce OLCs – However, recently viable methods such as the heating of nano-diamond could produce OLCs in large quantities.

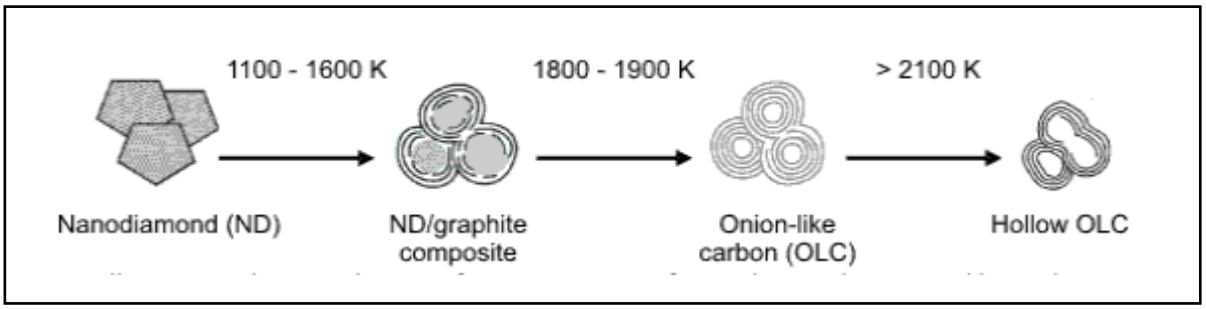

Figure 9: Making OLCs from Nanodiamonds [9]

2.4.3. Cerium Oxide (CeO_2)

Almost all electro-catalysts seem to degrade over their lifetime. Some leach into the electrolyte while others leach into the GDEs. For this reason, cerium oxide has been chosen to stabilize the catalyst and decrease the rate of degradation. CeO_2 will be fused with all electro-catalyst synthesized in this project to increase the life-span of the catalyst and/or AGFCS. A previous experiment and report showed that hydrogen and CO oxidation activity was significantly dependent on the cerium concentration [1]. A large concentration would increase activity and selectivity of the desired product H_2O but too much would lower the surface area of the catalyst and thus lower overall activity. They concluded that CeO_2 was a promising additive to PEMFCs [26].

References – Literature Review

1. Zhang, J. 2008. PEM fuel cell electrocatalysts and catalyst layers. *London: Springer*

2. Gasteiger, H., Kocha, S., Sompalli, B. & Wagner, F. 2005. Activity benchmarks and requirements for Pt, Pt-alloy, and non-Pt oxygen reduction catalysts for PEMFCs. *Applied Catalysis B: Environmental*. 56(1-2):9-35. DOI: 10.1016/j.apcatb.2004.06.021.

3. Modjtahedi, A., Amirfazli, A. &Farhad, S. 2016. Low catalyst loaded ethanol gas fuel cell sensor. *Sensors and Actuators B: Chemical*. 234:70-79. DOI: 10.1016/j.snb.2016.04.108.

4. News24. 2020. SA One Of The Worst In Alcohol-Related Road Deaths. [online] Available at: <http://www.news24.com/SouthAfrica/News/sa-one-of-the-worst-in-alcohol-related-road-deaths-20151203> [Accessed 14 October 2017].

5. Who.int. 2020. Road Traffic Injuries. [online] Available at: <http://www.who.int/mediacentre/factsheets/fs358/en/> [Accessed 4 January 2018].

6. Holton, O. & Stevenson, J. (2013). The Role of Platinum in Proton Exchange Membrane Fuel Cells. *Platinum Metals Review*. 57(4):259-271. DOI: 10.1595/147106713x671222.

7. Ito, S., Chibana, C., Nagashima, K., Kameoka, S., Tomishige, K. &Kunimori, K. (2002). CO hydrogenation over $RhVO_4/SiO_2$, Rh/V_2O_3 and Rh/SiO_2 catalysts: reduction and regeneration of RhVO4. *Applied Catalysis A: General*. 236(1-2):113-120. DOI: 10.1016/s0926-860x(02)00283-1.

8. Liu, Z., Gan, L., Hong, L., Chen, W. & Lee, J. 2005. Carbon-supported Pt nanoparticles as catalysts for proton exchange membrane fuel cells. *Journal of Power Sources*. 139(1-2):73-78. DOI: 10.1016/j.jpowsour.2004.07.012.

9. Chai, G., Yoon, S., Yu, J., Choi, J. & Sung, Y. (2004). Ordered Porous Carbons with Tunable Pore Sizes as Catalyst Supports in Direct Methanol Fuel Cell. *The Journal of Physical Chemistry B*. 108(22):7074-7079. DOI: 10.1021/jp0370472.

10. Jiang, J. &Kucernak, A. 2002. Nanostructured platinum as an electrocatalyst for the electrooxidation of formic acid. *Journal of Electroanalytical Chemistry*. 520(1-2):64-70. DOI: 10.1016/s0022-0728(01)00739-2.

11. Breeze, P. *et al* (2009). Renewable energy focus handbook. *Amsterdam: Academic Press/Elsevier*. ISBN: 9780123747051

12. LaConti AB, Hamdan M, McDonald RC. Mechanisms of chemical degradation. In. Handbook of fuel cells: fundamentals, technology, and applications, vol. 3. Vielstich W, Lamm A, Gasteiger H, editors. Chicester, *England: John Wiley and Sons*; 2003;647–62

13. Vingmed.se. 2020. [online] Available at: <https://www.vingmed.se/wp-content/uploads/2014/03/Broschyr_EN.pdf> [Accessed 23 October 2019].

14. Vij, V., Sultan, S., Harzandi, A., Meena, A., Tiwari, J., Lee, W., Yoon, T. and Kim, K., 2017. Nickel-Based Electrocatalysts for Energy-Related Applications: Oxygen Reduction, Oxygen Evolution, and Hydrogen Evolution Reactions. *ACS Catalysis*, 7(10), pp.7196-7225.

15. Jones, A. & Andersson, L. (1996). Variability of the Blood/Breath Alcohol Ratio in Drinking Drivers. *Journal of Forensic Sciences*. 41(6):14025J. DOI: 10.1520/jfs14025j.

16a. Zuba, D. (2008). Accuracy and reliability of breath alcohol testing by handheld electrochemical analysers. *Forensic Science International*. 178(2-3):e29-e33. DOI: 10.1016/j.forsciint.2008.03.002.

16b. Lamy, C., Rousseau, S., Belgsir, E., Coutanceau, C. & Léger, J. (2004). Recent progress in the direct ethanol fuel cell: development of new platinum–tin electrocatalysts. *Electrochimica Acta*. 49(22-23):3901-3908. DOI: 10.1016/j.electacta.2004.01.078.

17. Bianchini, C. & Shen, P. (2009). Palladium-Based Electrocatalysts for Alcohol Oxidation in Half Cells and in Direct Alcohol Fuel Cells. *Chemical Reviews*. 109(9):4183-4206. DOI: 10.1021/cr9000995.

18. Ahn, S. and Manthiram, A., 2017. Direct growth of ternary Ni–Fe–P porous nanorods onto nickel foam as a highly active, robust bi-functional electrocatalyst for overall water splitting. *Journal of Materials Chemistry A*, 5(6), pp.2496-2503.

19. You, B., Jiang, N., Sheng, M., Bhushan, M. and Sun, Y., 2015. Hierarchically Porous Urchin-Like Ni2P Superstructures Supported on Nickel Foam as Efficient Bifunctional Electrocatalysts for Overall Water Splitting. *ACS Catalysis*, 6(2), pp.714-721.

20. Furuya, N. and Motoo, S., 1978. The electrochemical behaviour of ad-atoms and their effect on hydrogen evolution. *Journal of Electroanalytical Chemistry and Interfacial Electrochemistry*, 88(2), pp.151-160.

21. Lin, R., Cao, C., Zhang, H., Huang, H. & Ma, J. (2012). Electro-catalytic activity of enhanced CO tolerant cerium-promoted Pt/C catalyst for PEM fuel cell anode. *International Journal of Hydrogen Energy*. 37(5):4648-4656. DOI: 10.1016/j.ijhydene.2011.05.021.

22. HALL, S. (2004). Influence of metal?support interaction in Pt/C on CO and methanol oxidation reactions. *Solid State Ionics*. 175(1-4):809-813. DOI: 10.1016/j.ssi.2004.08.030.

23. Sen, F. &Gökağaç, G. (2007). Different Sized Platinum Nanoparticles Supported on Carbon: An XPS Study on These Methanol Oxidation Catalysts. *The Journal of Physical Chemistry C*. 111(15):5715-5720. DOI: 10.1021/jp068381b.

24. Cao GZ. Nanostructures & nanomaterials: synthesis, properties & applications. *Singapore: World Scientific Publishing*, 2004.

25. Wang, X., Waje, M. & Yan, Y. 2005. CNT-Based Electrodes with High Efficiency for PEMFCs. *Electrochemical and Solid-State Letters*. 8(1):A42. DOI: 10.1149/1.1830397.

26. Miller, H., Lavacchi, A., Vizza, F., Marelli, M., Di Benedetto, F., D'Acapito, F., Paska, Y. & Page, M. et al. (2016). A Pd/C-CeO_2 Anode Catalyst for High-Performance Platinum-Free Anion Exchange Membrane Fuel Cells. AngewandteChemie International Edition. 55(20):6004-6007. DOI: 10.1002/anie.201600647.

27. En.wikipedia.org. 2020. Alkaline Fuel Cell. [online] Available at: <https://en.wikipedia.org/wiki/Alkaline_fuel_cell#/media/File:Alkalinecell.svg> [Accessed 18 February 2018].

3. Methodology

Chemicals

Cerium Nitrate ($Ce(NO_3)_3$)

Carbon Black (CB)

Onion-Like Carbon (OLC)

Ultrapure Water (UPW)

Palladium (Pd) nanoparticles

Nickel Chloride ($NiCl_2$)

Stirrer used: Stuart SB 162 heat-stir

Making the ink

1) In small vial, weigh 2mg of catalyst powder

2) Add 2uL of Nafion and 1mL of absolute (99%) ethanol

3) Sonicate for 1 hour

4) Mix contents using a pipette.

Experimental solutions (100mL)

KOH

0,5M KOH = 2.81g KOH + 100ml Ultrapure Water (UPW)

KOH (+Ethanol) [1:1] (Ethanol Specific Energy = 8.0kWh/kg)

1M KOH + 1M EtOH = [2.81 KOH + 50ml UPW] + [2.95mL EtOH (99.9%) + 47.05mL UPW]

Ferric-Ferrocyanide (1:1) in 0.1M KCl

0.03:0.03:1 = 0.127g $K_4(CN)_6.3H_20$ + 0.099g $K_3(CN)_6$ + 0.746g KCl + 100mL UPW

Table 2: Catalysts For This Research Project

CORE METAL(S)	
Palladium (Pd)	Palladium (Pd)
Palladium-Nickel (PdNi)	Palladium-Nickel (PdNi)
SUPPORTS	
CB	OLC
CeO_2/CB	CeO_2/OLC

CATALYSTS SYNTHESISED FOR RESEARCH		
CB catalysts (A)	**Concentrations**	**OLC catalysts (B)**
1A) Pd/CB	[10:90]	1B) Pd/OLC
2A) PdNi/CB	[10:10:80]	2B) PdNi/OLC
3A) Pd/CeO_2-CB	[10:90]	3B) Pd/CeO_2-OLC
4A) PdNi/CeO_2-CB	[10:10:80]	4B) PdNi/CeO_2-OLC

3.1. Synthesising the Supports CeO_2/CB (and CeO_2/OLC)

1) Add 1.507g of Cerium Nitrate to 50ml of Ultrapure Water (UPW) in a conical flask

2) Slowly add 1.130g CB (or OLC) to cerium nitrate slurry

3) Fill to 100ml with UPW ensuring to wash the walls of the flask

4) Stir for 30mins

5) In another flask, make 40ml of 2M KOH – stir for 10mins

6) Add mixture (5) to (3) until a pH of 12 is achieved

7) Sonicate for 1 hour

8) Stir vigorously for 2 hours

9) Centrifuge and wash to pH 7

Yield after step 9: CeO_2/CB = 2.0091g

CeO_2/OLC = 2.0225g

10) Using a furnace, heat 1.700g CeO_2/CB (or CeO_2/OLC) to 250^oC for 3 hours

11) Cool to room temperature (25^oC) under a flow of Argon (Ar)

3.2. Synthesising the Catalysts

Table 3: Synthesising The Catalysts

Mono-metal Pd	**Bi-metal PdNi**
1) Add 0.3333g of support to 50mL of UPW in a round bottom flask 2) Stir vigorously (1150rpm) for 30 minutes 3) In a vial, add 0.1150g K2PdCl4 to 5mL UPW 4) Sonicate both for 30 minutes 5) Stir support for another 10 minutes 6) Using a pipette, mix Pd solution for 2mins and sonicate for another 8mins 7) Wash walls of flask with UPW (5mL max) 8) Add Pd solution dropwise (30drops/min) under stirring @ 1000rpm 9) Stir for 20mins 10) Prepare 2.5M KOH solution and 99% (absolute) ethanol 11) Add 0.7mL of KOH followed by 4.2mL ethanol 12) Heat under reflux @ 80^oC for 1 hour 13) Add water to 250mL and leave to cool for 10mins 14) Centrifuge and wash to neutral	1) Add 0.2958g of support to 45mL of UPW in a round bottom flask 2) Stir vigorously (1150rpm) for 30 minutes 3) In a vial, add 0.1150g K2PdCl4 and 0.1519g $NiCl_2 \cdot 6H_2O$ to 10mL UPW 4) Sonicate both for 30 minutes 5) Stir support for another 10 minutes 6) Using a pipette, mix PdNi solution for 2mins and sonicate for another 8mins 7) Wash walls of flask with UPW (5mL max) 8) Add PdNi solution dropwise (30drops/min) under stirring @ 1000rpm 9) Stir for 20mins 10) Prepare 2.5M KOH solution and 99% (absolute) ethanol 11) Add 1.4mL of KOH followed by 8.4mL ethanol 12) Heat under reflux @ 80^oC for 1 hour 13) Add water to 250mL and leave to cool for 10mins 14) Wash to neutral and vacuum/gravity filter overnight

4. Characterisation Techniques Used

4.1. X-ray Diffraction Analyses (XRD)

Why

XRD is an instant output experiment. The primary use of XRD is to identify the phases in your powdered compound. If the output is "fuzzy" beyond other justification, it can be deduced that the material is amorphous. However, if the reading is clear, phase identification is rather simple and the user can the atomic spacing between the different atoms present in the tested compound – especially when the user already knows the composition of the material.

How

The machine (Figure 10b) consists of 3 key components: a) Sample Holder b) X-ray Tube c) X-ray Detector.

The user should finely ground (powedered) their sample to be tested. If this is not done correctly, the holder cannot be packed properly and the xray beams could react to the "clumps" and output incorrect peaks. The sample holder (Figure 10a) should be carefully cleaned using a tissue and acetone as this removes impurities left behind from the previous experiments. There are 2 methods of packing (side and top) with top packing being the predominant method. This involves pouring the material in the concentric circles found at the centre of the holder. Covering the material and holder with a glass sheet and gently tapping, turning the system sideways and tapping, and other forms of gently settling the powder are acceptable. The holder should be cleaned of all residual material and the sample should not exceed the height of the holder (i.e. should not spill out of the grooves). Once gently placed in the machine, the sample is hit with X-rays and produces both a defracted ray and constructive interference - when the conditions satisfy Bragg's Law ($n\lambda=2d \sin \theta$) which relates the resulting wavelength to the diffraction angle and spacing of the lattice [1]. This is done at an angle of 2θ – it is general practice that the wider the angle the better as it accounts for random orientations of the sample.

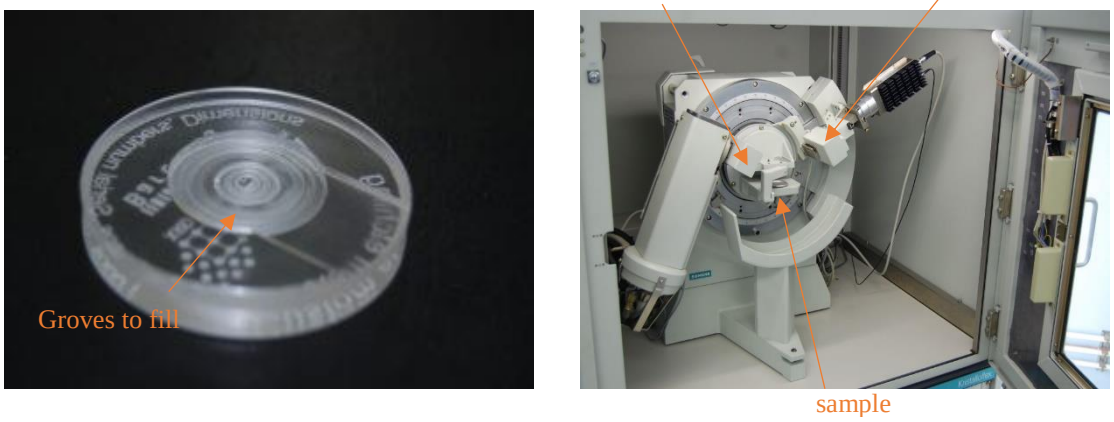

Figure 10: XRD (a) sample holder and (b) tesing platform[1]

PS. The XRD machine used for this research used Cobalt (Co) as the reference material. Using the equation below, the results are altered to be based on using Copper (Cu) as the reference.

$$Cu(2\Theta) = 2\text{Asin}\left[sin\left(\frac{2A\pi}{2*180}\right)*\frac{1.54056}{1.7891}\right]*\frac{180}{\pi}$$

4.2. Scanning Electron Microscopy (SEM)

Why

SEM images along with TEM and other similar techniques are a means to view your material at a microscopic level. SEM is used (along with EDS – Energy Dispersive Spectroscopy) to identify the different elements in the material. It not only verifies the existence of what was used to make the material but also gives an idea at the concentrations of each (this part is given by EDS). The surface morphology is indicated by and visualised due to the varying denistiers of the compounds.

How

The first step is to determine whether or not the sample needs to be coated (in gold for example) or the material has sufficient conductivity. Then 2-sided carbon tape is used to stick the sample to a small stub that will be gently placed in the machine. The magnification levels vary from machine to machine but 50-100µm are commonly found in schools and research facilities alike.

The greater the zoom, the slower the scanning rate so as to not lose contrast. As opposed to XRD which fired xrays, SEM fires beams of high-energy electrons that on the sample in a vacuum chamber. Low energy electrons are then emitted from the sample (the sample would absorb and release different energy levels of electrons. The variations in the secondary (low energy) electrons appear on screen as a contrast where dense atoms appear as "whitish" while the less density atoms appear dark grey or black. This allows the user to track the surface morphology of their sample (how it is spread) and the EDS provides the incite into their concentrations.

4.3. Thermogravimetric Analyses (TGA)

WHY

TGA is a destructive analyses technique (the sample is not usable afterwards). TGA is another means to verify and/or validate the contents in the sample. It gives insight into the purity of your sample. TGA also helps identify the ignition and drying temperatures of the product and provides an indication for safe operating conditions when using the product elsewhere.

HOW

The TGA is one of the most simple yet effective techniques available. A material is placed in a mini furnace and gradually heated from room temperature up to (for our research) 950^{o}C. The machine is fitted with a scale and operates in a vacuum. The gradual heating results in atoms vapourising and leaving the sample which in turn decreases the weight of the sample. Tracking the changes in mass and the temperature at which it happens, gives insight to the structural make-up, mass concentration, and the factors mentioned previously.

Figure 11: Entry level TGA equipment[2]

4.4. Brunauer Emmett Teller (BET)

WHY

BET is an analyses technique that helps us understand the specific (physical) area of the samples. Factoring the pores and other surface imperfections BET would tell us the pore volume, BET surface area, and pore width. Which can directly be translated to the structural behaviour of the catalysts – as seen in section 5 below - by giving insight into the fundamentals of gas adsorption molecules onto the surface of the solid.

HOW

The principles behind the BET analyses are rather simple to understand compared to other techniques discussed in this report and is based on the formula below [3].

$$\frac{P}{V(Po - P)} = \frac{1}{Vm * C} + \frac{P(C - 1)}{Po(Vm * C)}$$

Where;

P = Equilibrium pressure

P_o = Saturated Vapour Pressure

V = Total Volume of Molecules Added

V_m = Volume of Gas Molecules Corresponding to the Monolayer

Zhang *et al* [1] phrased it best when they said that BET essentially uses the surface of adsorbed molecules as a ruler. We know the size of atoms through previous studies. Thus all that needs to be done is determining how many of the molecules would fit on the surface of the sample being analysed (the monolayer mentioned in the equation). This is done by exposing the sample to different amounts of gas and measure the pressure in the chamber – the pressure decreases as gas is adsorbed onto the surface. The 2 underlying assumptions are that the gas molecules cause negligible interactions with each other and that only one gas molecule can occupy a site on the surface (minimal or no overlap). Varying the amount of gas in the chamber alters the equilibrium pressure – this knowledge together with the equation above can tell you about the surface area of the sample by solving for V_m.

4.5. Raman Specroscopy Analyses (RSA)

WHY

Raman is an essential tool to observe the structure (especially defects) and disorder nature of a material. It provides and insight into the vibrational and rotational states of the system in question. The peaks formed in RSA could be thought of as a fingerprint of the material as no two measurements would be exactly alike. Key outputs of RSA are confirming the doping and/or crystallinity of the material and the bond lengths present. This is complementary to Infrared Specstroscopy (IRS) as IR-active bonds will not be Raman-active and vice-versa for symmetrical molecules hosting a centre of inversion [4].

HOW

The laser of monochromatic light is fired at the sample. The light is absorbed my the molecules present increasing it's internal energy causing the molecule to jump to a higher rotational (or vibrational energy level – see diagram below). When the molecule relaxes and goes back to a lower energy level but not necessarily the same as before, it releases the radiation at a different frequency as that of the incident ray. If the radiation emitted has a lower frequency that the original (incident) beam, it is referred to as Stokes scattering and when it has a higher frequency, it is referred to as anti-Stokes scattering. This effect is graphed as intensity peaks detected in the system. Comparing the area of the peaks (for this report, peak 1 represent Pd and peak 2 represent Pd-O) tells us the level of doping that has occurred. The ratio of the defect factor and crystalline factor (I_d/I_g) informs us of the defects of the material where a value less than 1 represents little or low defects and/or doping.

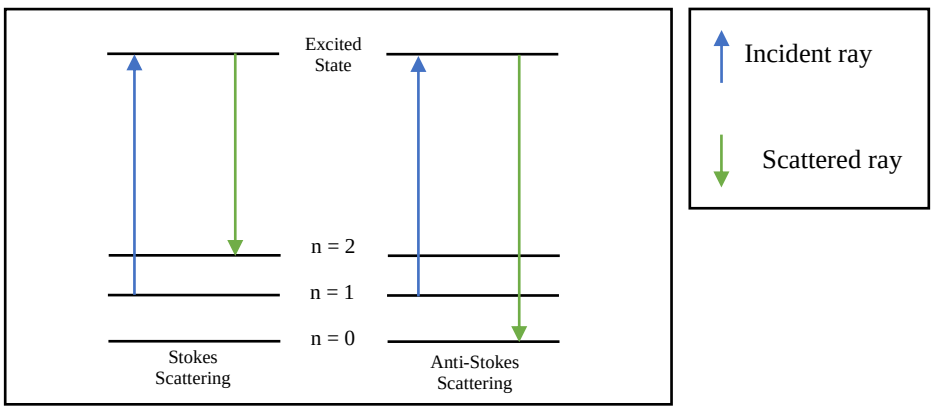

Figure 12: Stokes and Anti-Stokes Scattering

5. Electrochemical Techniques Used

All techniques required the electrolyte solution to first be purged with Nitrogen prior to the commencement of the experiment. The details and conditions were mentioned in chapter 3

5.1. Cyclic Voltammetry (CV)

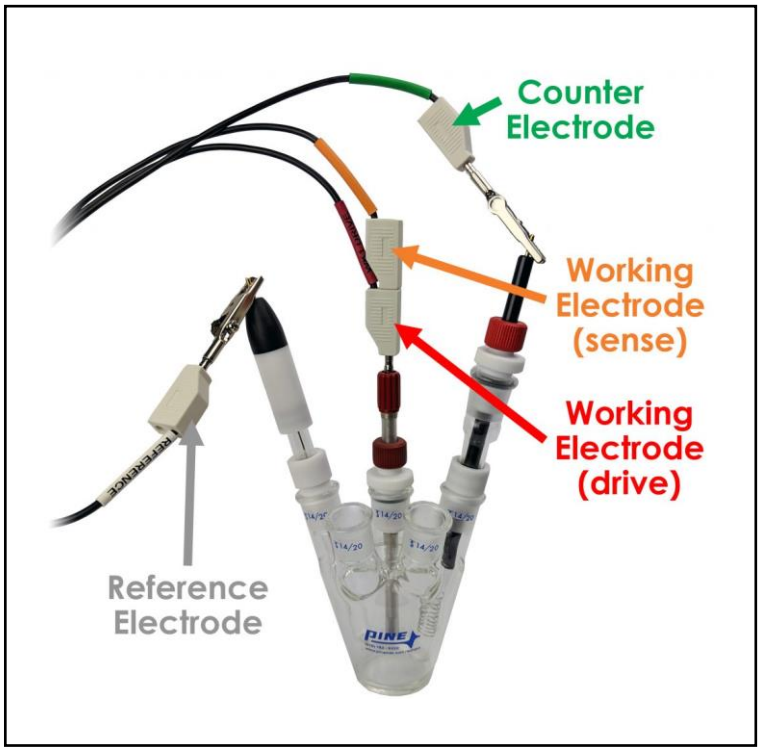

Figure 13: 3-Electrode System Used For The Electrochemical Techniques [5]

5.1.1. In KOH

WHY

Performing the CV in KOH allows us to get an understanding of the ECSA present in the catalyst. While BET provides the physical surface area, ECSA is the area that is active during the process and would thus be slightly lower due to the support or impurities blocking the OH^- from reaching the Palladium (or any other) catalyst core. This value is largely dependent on the support material used.

HOW

$$ECSA = \frac{Q}{S.L}$$

Where, Q = Integral of hydrogen adsorption from CV plot,

S = Charge density constant for Pd (0.424 mC/cm^2), and

L = mass loading of Pd on electrode.

Using the above equation, the ECSA can be calculated. Q is obtained from using an analysing software such as EC-Lab and measuring the area of the / integrating the adsorption desorption peak. S is a constant for the material in question and can be found from previous literature and L can be found by measuring the electrode before and after coating it with the catalyst or converting the volume of catalyst applied to the electrode into mass accounting for the solution vapourisation.

5.1.2. In KOH+EtOH

WHY

Forming the crux of the project, performing the CV in Potassium Hydroxide and Ethanol simulates "human breath". This informs us of the capabilities of the catalyst to detect ethanol and generate a current. Varying the concentrations and conditions of this experiment (such as scanning rates) allows multiple outputs from this setup such as sensitivity and reliability.

HOW

The diffusion coefficient of the material can be obntained by taking an output matrix of the current density and the root of various scan rates. Plotting this would result in a straight line with the gradient expanded by the Randell Sevcik equation which at 25^{o}C simplifies to [6]:

$$ip = \overbrace{\boxed{2.69 * 10^5 * n^{\frac{3}{2}} * A * D^{\frac{1}{2}} * C}}^{\text{Gradient}} * v^{\frac{1}{2}}$$

I_p = Peak Current in Amps

n = Number of Electrons Transferred

A = Electrode Area in cm^2

D = Diffusion Coefficient in cm^2/s

C = Concentration in mol/cm^3

ν = Scan Rate in V/s

Another useful output is looking at the onset potential of the CV plots (no calculation required) which tells us the energy required to start the reaction as well as the peak-to-peak ratio which relates the oxidation and reduction steps.

5.2. Linear Sweep Voltammetry (LSV)

WHY

It informs us by how much we need to increase the overpotential in order to increase the reaction rate tenfold. Tafel extrapolation also provides insight into the corrosion susceptibility of the catalyst which speaks about it's relaibiltity and durability alike.

HOW

LSV is a slow experiment and in this research conducted at 1mV/s. The LSV data is transformed into tafel plots by plotting the Log_{10}(current density) vs the net potential (actual potential – the potential of the reference Ag/AgCl(saturated) electrode i.e. 0.197V). The gradient of this straight line plot is the tafel value required.

5.3. Electrochemical Impedence Spectroscopy (EIS)

WHY

EIS is and electrochemical technique used to measure the resistance (impedence) of a system. The EIS along with the techniques mentioned previously aid in determining the pathway and rate of the reaction. EIS informs the individual of both the solution resistance as well as that of the catalyst itself.

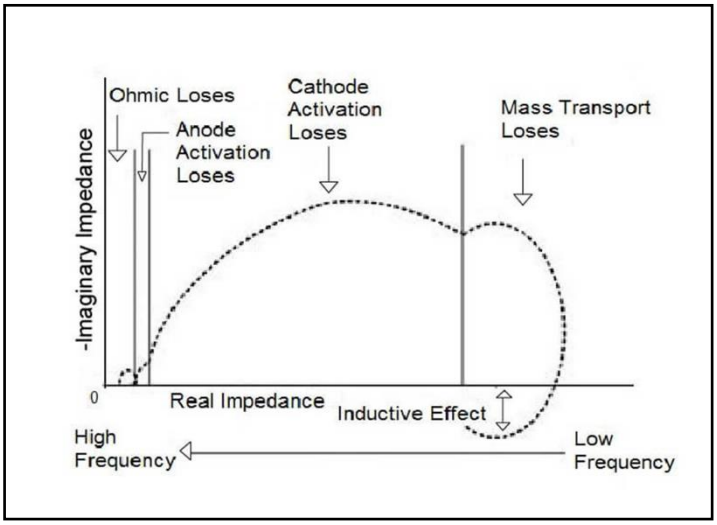

Figure 14: EIS Zones [3]

HOW

The EIS set-up is unique in the sense that the counter electrode depicted in Figure 13 is no longer attached and thus essentially forms a 2-electrode system.

After setting up the initial parameters and letting the experiment run. The EIS plots in chapter 6 are obtained plotting the imaginary and real resitances (in Ohms). The key elements under observation for this project were the ohmic and anode activation losses labelled above. An example circuit is selected (or created) in EC-Labs in order to model the system as an electric cicuit. The pseudo capacitance can be determined after fitting and can be found at the end of chapter 6. The calculations and Z-fit are run for 10 000 iterations to minimize deviations during the fitting process.

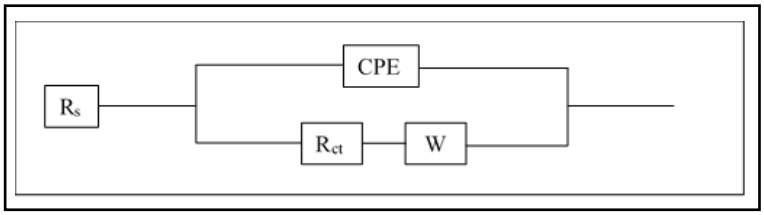

Figure 15: Circuit Fitting for EIS Data

References – Techniques Used

1. Edwards, A., 1975. H.P. Klug and L.E. Alexander, x-ray diffraction procedures for polycrystalline and amorphous materials. Analytica Chimica Acta, 77, p.349.

2. TA Instruments. 2020. Thermogravimetric Analyzers. [online] Available at: <https://www.tainstruments.com/products/thermal-analysis/thermogravimetric-analysis/> [Accessed 7 April 2020].

3. Zhang, J. 2008. PEM fuel cell electrocatalysts and catalyst layers. *London: Springer*

4. Sas.upenn.edu. 2020. Raman Spectroscopy. [online] Available at: <https://www.sas.upenn.edu/~carrolld/SpecProjectPages/Raman.html> [Accessed 2 August 2019].

5. Pine Research Instrumentation Store. 2020. Three-Electrode Setups. [online] Available at: <https://pineresearch.com/shop/kb/applications/rde-and-rrde/three-electrode-setups/> [Accessed 18 December 2019].

6. Holze, R., 2002. Book Review: Electrochemical Methods. Fundamentals and Applications (2nd Edition). By Allen J. Bard and Larry R. Faulkner. Angewandte Chemie International Edition, 41(4), pp.655-657.

6. Result and Discussions

The research, although involving 8 catalysts, has been broken down into 2 sub-projects each containing 4 catalyst. This is done for clarity and should be easier to digest for any reader. Thus, some wording might overlap during the consolidation of the 2 sub projects – please excuse this.

In ethanol oxidation reaction (EOR) various strongly adsorbed intermediate such as acetic acid, acetaldehyde, and carbon monoxideused to form, which can poison the electrocatalytic surface and reduced the ethanol oxidation efficiency [15]. On the other hand, in alkaline fuel cell adsorption of OH^- on the catalyst surface leads to the poisoning of the catalyst surface. However, Ni would activate the dissociation of a water molecule (H_2O ---→ $H^+ + OH_{ads} + e^-$) at lower potential and provide an active site for the OH adsorption [16]. Hence, the alloy formation of Pd with Ni can protect the active site of the Pd surface from the adsorption of OH^- and the ethanol oxidation efficiency of the PdNi would be expected to increase. Therefore, in the present report PdNi alloy used as an anode electrode for the EOR.

After the first report involving the monometallic Pd-Core and validating that the carbon support helps to transfer the electron from the electrocatalyst to the support, we have used the various carbon support for the PdNi catalyst as well. Cerium oxide is a support that could help stabilise the catalyst and is thus tested as well [21]. The project could thus be viewed as a 3 part comparison: Monometallic vs Bimetallic core catalysts, OLC vs Carbon Black, and Cerium-Oxide supported vs Ceria-free catalysts.

6.1. Material Structure Analysis

6.1.1. X-ray Diffractions (XRD)

6.1.1.1. Monometallic Core (Pd)

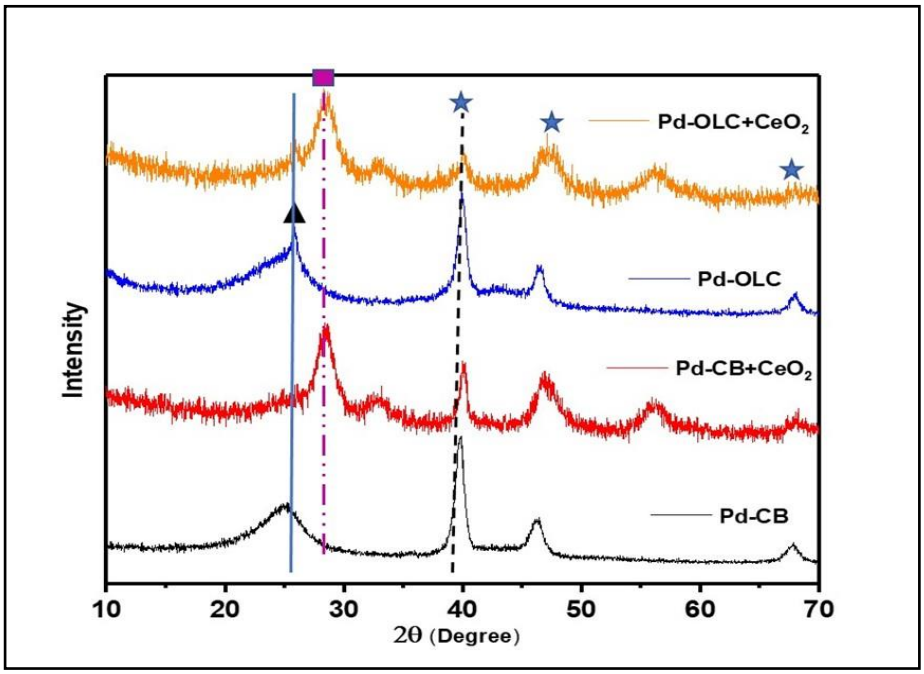

Figure 16: XRD spectrum of the Various Pd Catalysts

As-prepared electrocatalyst has been characterized by XRD, SEM, TGA, BET, and Raman spectroscopy. The XRD patterns of Pd-CB, Pd-CB+CeO_2, Pd-OLC, and Pd-OLC+CeO_2 are shown in Figure 16. XRD pattern of Pd/CB possesses a broad peak at approximate 24º, which is corresponding to 002 planes of graphitic carbon with a low degree of graphitization. Moreover, the Pd-OLC shows the sharp peak at the top of the broad peak at approximate 24º, corresponding to the higher degree of graphitization compared to the CB. The graphitized carbon of Pd-OLC may help for the enhancement of electrochemical activity and stability. Since graphitized carbon possesses good conductivity along with corrosion resistance property.

Further, in the case of Pd-CB+CeO_2 and Pd-OLC+CeO_2 the carbon peak (CB and OLC) has been suppressed, and the new peak near 28º observed and shown by the square in Figure 16. The newly obtained peak was observed and it assignsto the CeO_2. Along with the carbon and CeO_2, the Pd peak for Pd-CB, Pd-CB+CeO_2, Pd-OLC, and Pd-OLC+CeO_2 was found and shown by star symbol in the XRD spectrum. Among all the as-prepared catalyst Pd-OLC shows

the very sharp peak of the Pd, it attributed to the crystalline Pd particles on the OLC. The highly graphitized carbon and the crystalline Pd of the Pd-OLC, is expected to showthe superior electrochemical performance among all the as-prepared catalyst.

6.1.1.2. Bimetallic Core (Pd+Ni)

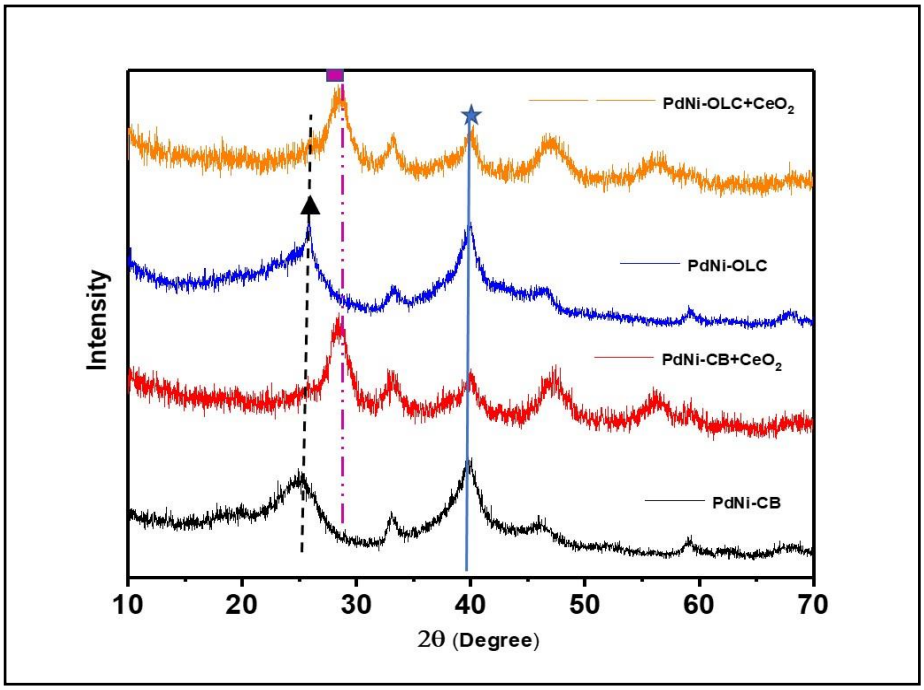

Figure 17: XRD spectrum of the Various PdNi Catalysts

Figure 17 shows the XRD patterns of PdNi-CB, PdNi-CB- CeO_2, PdNi-OLC, and PdNi-OLC-CeO_2. XRD pattern of PdNi-CB possesses a broad peak at approximate 24^o, which is corresponding to 002 planes of graphitic carbon. Whereas, PdNi-OLC shows a sharp peak on top of the broad peak at 24^o, corresponds to graphitic carbon. Hence, CB possess the non-graphitic carbon, however, OLC suggests the graphitic carbon. The carbon peak in Figure 17 shown by the triangle symbol and the square symbol at 28^o suggest the CeO_2. The peak at 40^0 indicated Pd since the peak is not very sharp, and broadening of peak suggests the Ni incorporation in the crystal of Pd [17].

6.1.2. Scanning Electron Microscope (SEM)

6.1.2.1. Monometallic Core (Pd)

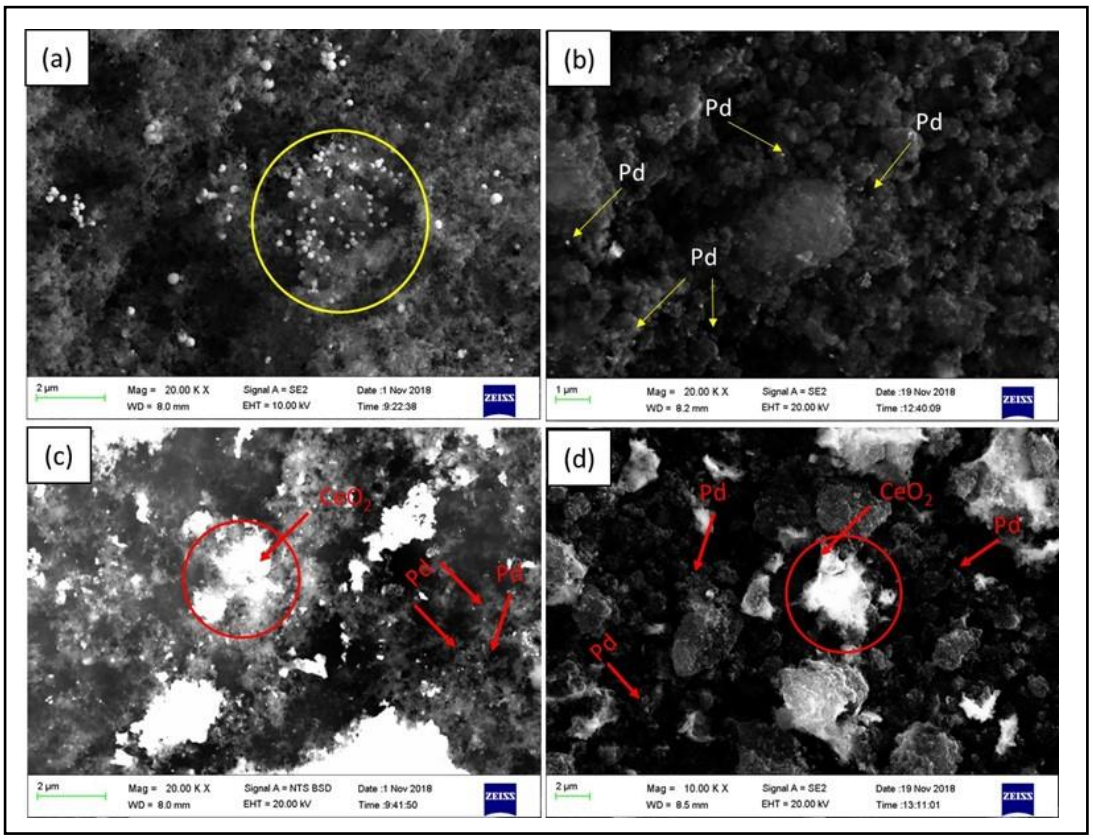

Figure 18: SEM images of the (a) Pd-CB (b) Pd-OLC, (c) Pd-CB+CeO_2, and (d) Pd-OLC+CeO_2

Further, to understand the distribution of Pd nanoparticles on various support, the morphology of the as-prepared Pd-CB, Pd-CB-CeO_2, Pd-OLC, and Pd-OLC-CeO_2 was obtained by scanning electron microscope (SEM) images and results are shown in Figure 18. Figure 18a represents the Pd-CB, and Pd particles are agglomerated and highlighted in the circle. It suggests that the Pd particles are not well dispersed throughout the CB surface. However, in Figure 18b of Pd-OLC indicates the uniform distribution of Pd particles on the OLC surface. Further, in the case of Pd-CB+CeO_2, the Pd particles are well distributed as shown in Figure 18c, but the CeO_2 shows the agglomerated on the CB surface shown in the circle. Moreover, Pd-OLC+CeO_2, CeO_2 on the OLC surface is less agglomerated comparatively CB as shown in Figure 18d.

6.1.2.2. Bimetallic Core (Pd+Ni)

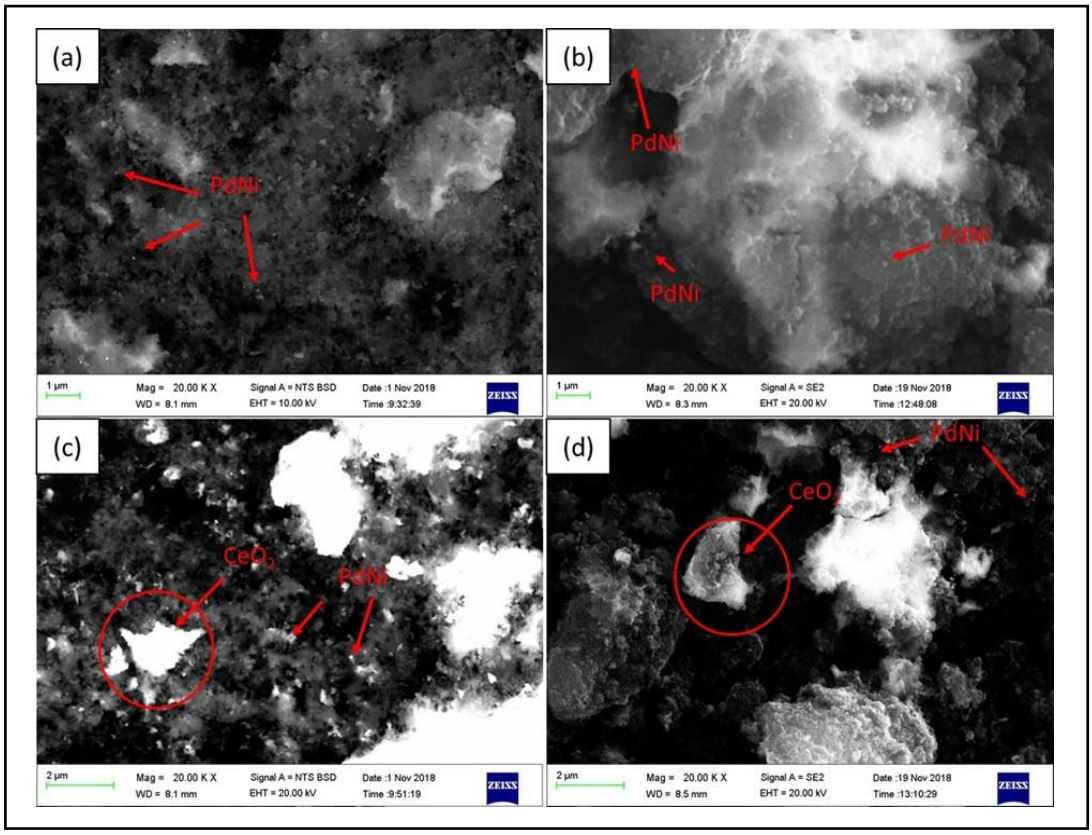

Figure 19: SEM images of the (a) PdNi-CB (b) PdNi-OLC, (c) PdNi-CB+CeO_2, and (d) PdNi-OLC+CeO_2

The morphology of the as-prepared electrocatalysts PdNi-CB, PdNi-CB+CeO_2, PdNi-OLC, and PdNi-OLC+CeO_2 is shown in Figure 19. The PdNi on CB are well dispersed and shown by the arrow in Figure 19a, however, PdNi particles on OLC also distribute and the size of the particles is lesser than the PdNi-CB shown in Figure 19b. Figure 19c and 19d shows the presence of CeO_2 and highlighted by the circle. It suggests that the CeO_2 well adsorbed on the CB and OLC in Figure 19c and 19d respectively. The well-dispersed PdNi particles may help to enhance the electrochemical performance.

6.1.3. Thermogrametric Analyses (TGA)

6.1.3.1. Monometallic Core (Pd)

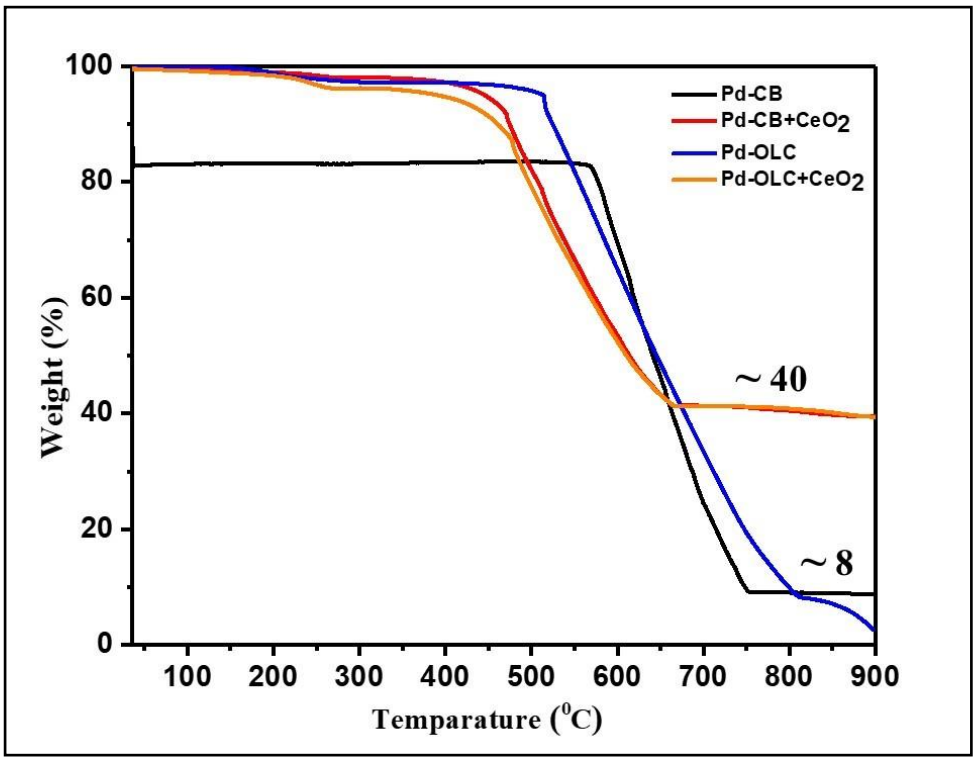

Figure 20: TGA Curves of the Various Pd Catalysts

Thermogravimetric analysis (TGA) was performed on the as-prepared catalyst to determine the amount of Pd catalyst on the support. The TGA analysis was conducted under the air atmosphere in the temperature range from room temperature (RT) to 900^0C. In this condition, the carbon can get the evaporate and the remaining residue is considered as the metal content. Figure 20 shows the TGA analysis of the as-prepared catalyst and Pd content is approximately 8% present in the Pd-CB and Pd-OLC. Further, metal content approximately 40% is present in the Pd-CB+CeO_2 and Pd-OLC+CeO_2, it includes the weight percentage of CeO_2 and Pd. The carbon evaporation of the Pd-CB and Pd-OLC shows at higher temperature comparatively Pd-CB+CeO_2 and Pd-OLC+CeO_2.

6.1.2.2. Bimetallic Core (Pd+Ni)

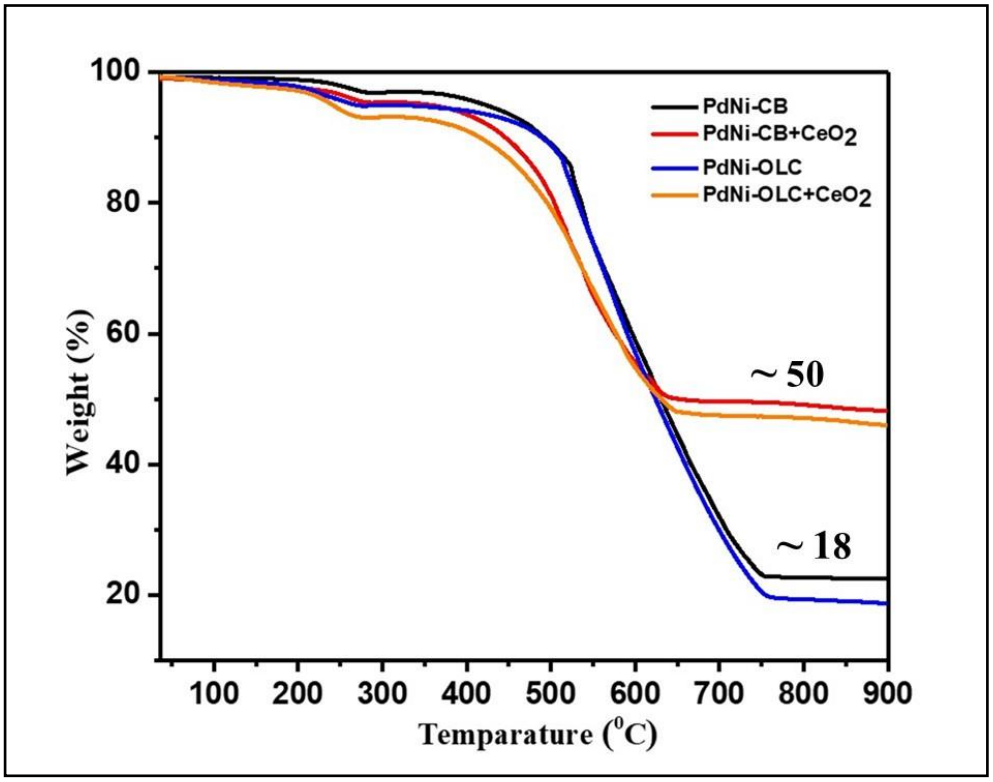

Figure 21: TGA Curves of the Various PdNi Catalysts

Thermogravimetric analysis (TGA) helps to estimate the metallic percentage in the as-prepared catalysts and is shown in Figure 21. Therefore, the TGA analysis was performed in air medium so the carbon can be evaporated the remaining residue can consider as the metallic part. The TGA analysis of PdNi-CB and PDNI-OLC shows the presence of the approximately 18% of a metallic content and 50% is present in the Pd-CB+CeO_2 and Pd-OLC+CeO_2. From the percentage of PdNi-CB, PdNi-CB+CeO_2, PdNi-OLC, and PdNi-OLC+CeO_2, it can estimate that around 30% is the CeO_2 and remaining carbon is present in the as-prepared catalysts.

6.1.4. Brunauer Emmett Teller (BET)

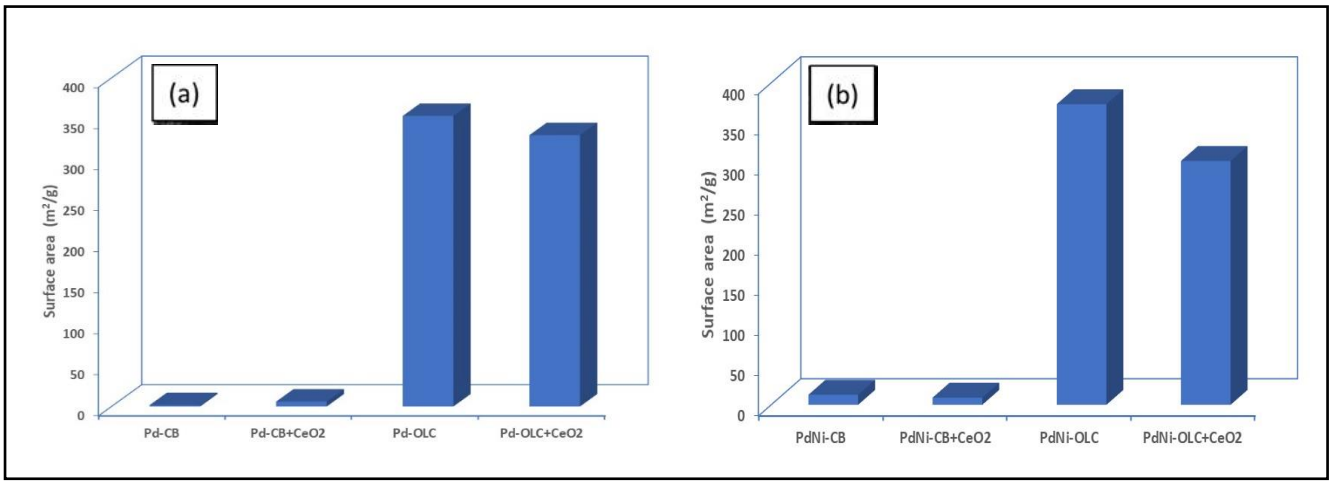

Figure 22:Comparison of surface area of ALL Catalysts

The Braunner-Emmett-Teller (BET) surface area of the as-prepared catalysts was compared in Figure 22a and 22b. Pd-OLC and PdNi-OLC show the highest surface area among all of the as-prepared catalyst. The Pd-OLC shows the highest surface area overall and this high surface area of the Pd-OLC can be helpful in the adsorption of ions from the electrolyte, and it can help to shorten the diffusion of ions [1].

The highest surface area is due to the OLC and it may help to faster kinetics during the ethanol oxidation reaction. The structure of the Onion-Like Carbon depicted earlier in the report show the myriad openings due to the spirallic nature of the material – this directly contributes to the significantyly higher surface areas when contrasting the two carbon based supports.

6.1.5. Raman Spectroscopy Analyses (RSA)

6.1.5.1. Monometallic Core (Pd)

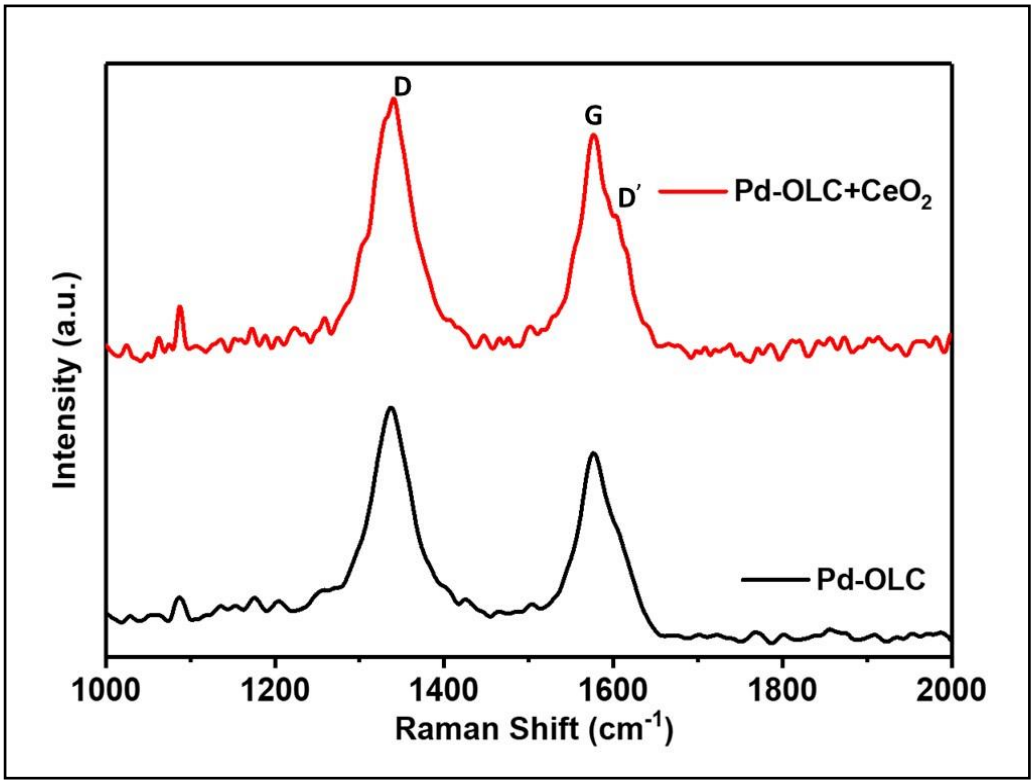

Figure 23: Raman Spectra of Pd-OLC and Pd-OLC+CeO

Raman spectroscopy is a non-destructive technique to understand the structure of carbon material. Hence, herein we have used the carbon and the metal oxide as support for the electrocatalyst of the ethanol oxidation reaction. Raman spectrum of the Pd-OLC and Pd-OLC + CeO_2 shown in Figure 23. The presence of D -band peak by the disordered structure of SP^2 hybridized carbon system, whereas, G-band arises is due to the E2g and exist due to the stretching of carbon-carbon bond in graphitic carbon. However, in the case of Pd-OLC+CeO_2 small peak at the G peak is observed and known as D'-peak, is due to the impurities or surface charges. It may occur due to the presence of CeO_2 on carbon network. The small peak at 1088 cm^{-1} for Pd-OLC and Pd-OLC+CeO_2 was observed and itsattributes to the presence of Pd. Further I_d/I_g ratios provide information about defects/disorder in the carbon materials.The I_d/I_g ratios of 1.20 and 1.12 were observed for the Pd-OLC and Pd-OLC+CeO_2, respectively [2].

6.1.5.2. Bimetallic Core (Pd+Ni)

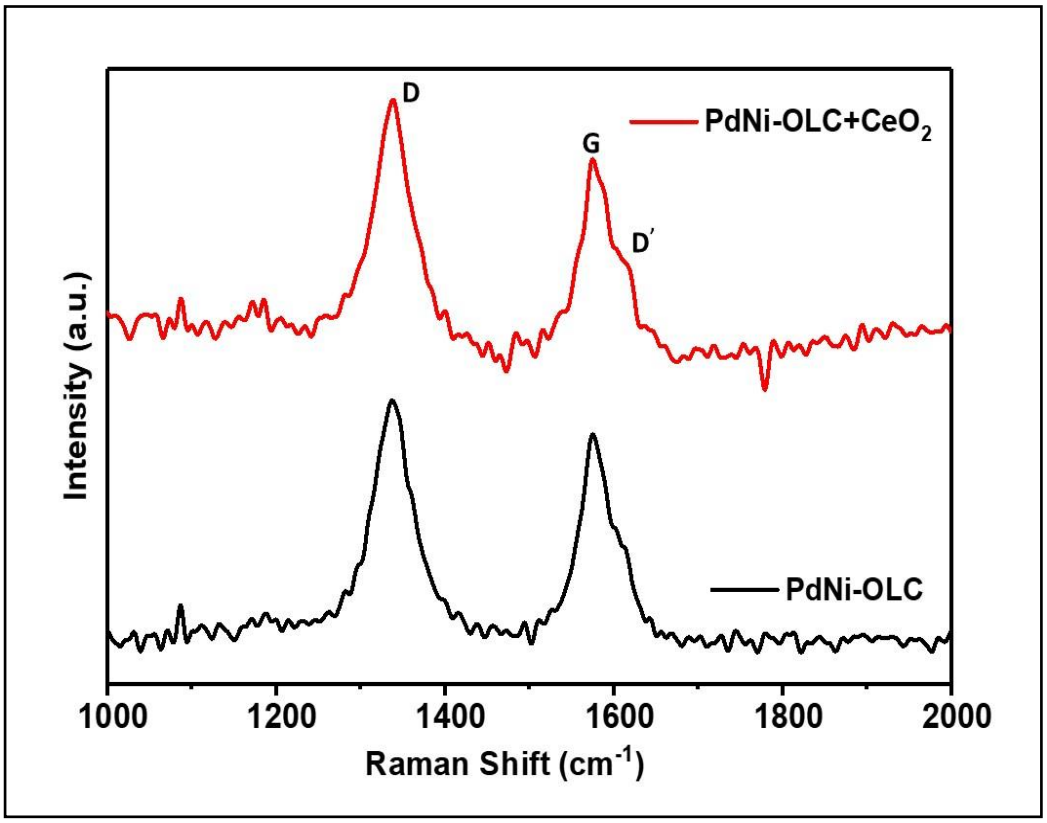

Figure 24:Raman Spectra of PdNi-OLC and PdNi-OLC+CeO_2

Carbon based material can be characterized by the Raman spectroscopy that has become a key technique for the analysis of different types of SP2 nanostructures. Figure 24 shows the Raman spectrum of the PdNi-OLC and PdNi-OLC+CeO_2. Disordered structure of the carbon system was confirmed by the presence D-band peak. G-band peak in figure 24 indicates the stretching of carbon-carbon bond in OLC [2] . However, G-peak split into the D' -peak and G peak , and it was observed for the PdNi-OLC+CeO_2 and D'-peak indicates the presence of CeO_2. The presence of Pd and Ni can be confirmed by the peak at 1088 cm-1 for PdNi-OLC and PdNi-OLC+CeO_2. The intensity ratios of the D and G-peak i.e. Id/Ig helps to estimate the defects in the carbon material [1]. The Id/Ig ratios of 1.18 and 1.13 were observed for the PdNi-OLC and PdNi-OLC+CeO_2, respectively. The higher Id/Ig ratio ensure more defects on carbon material.

6.2. Electrochemical Performance Analysis

6.2.1. Cyclic Voltammetry (CV) – FerroFerric

6.2.1.1. Monometallic Core (Pd)

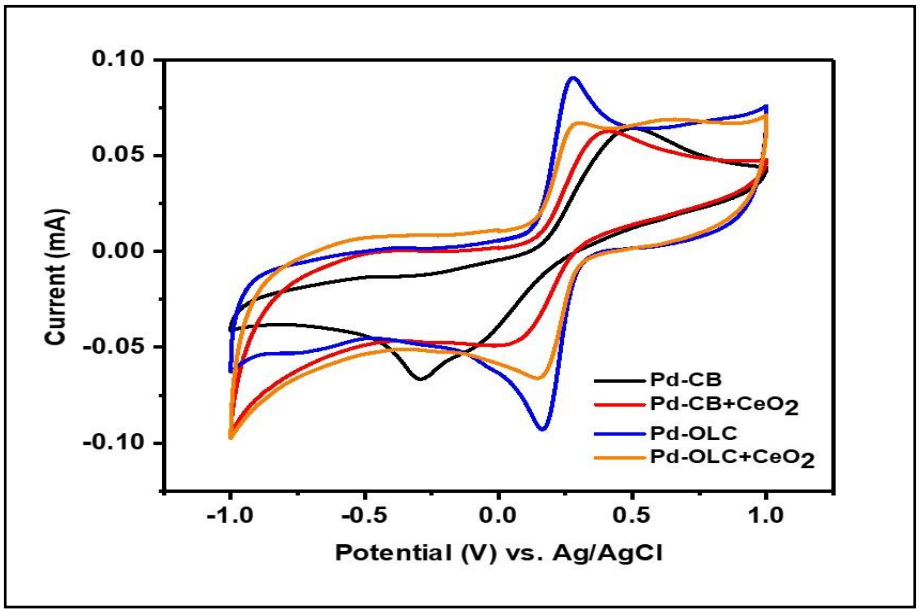

Figure 25: The CV for potassium ferrocyanide/potassium ferricyanide with scan rate of 50 mV/s of the Various Pd Catalysts

Carbon support plays a crucial role not only for the electrocatalyst distribution on carbon support; also, it promotes the electronic structure of the catalyst. Such as degree of graphitization, presence of surface functionalities, heteroatom (N, P, S, B) dopant in carbon matrix influence the electron transfer from electrocatalyst to support. Besides that, textural and morphological (porosity, surface area, etc.) of support affect the activity of electrocatalyst and selectivity of ethanol oxidation. Therefore, this project mainly focused on the support for the electrocatalyst [3, 4 5].

The cyclic voltammetry (CV) is the important techniques to understand oxidation and reduction peak for the redox reaction. As seen in Figure 25, anodic and cathodic scan proceed the oxidation of $K_4Fe(CN)_6$ to $K_3Fe(CN)_6$ and reduction is vice-versa as shown below.

$$K_4Fe(CN)_6 \leftrightarrow K_3Fe(CN)_6 + e^- \quad [1]$$

The CV curves of Pd-CB, Pd-CB+CeO_2, and Pd-OLC+CeO_2 shows the broad peak of oxidation and reduction and the sharp peak has appeared for the Pd-OLC in Figure 25. It suggests that the Pd-OLC possess high reversibility and fast kinetic for electrochemical performance. Hence, it is expected that the Pd-OLC could have the fast kinetics for ethanol electrooxidation reaction. It may occur due to the faster electron transfer from the catalyst surface to the support. This indicates that the OLC could be the good support for the fast electron transfer and better ethanol electrooxidation reaction.

6.2.1.2. Bimetallic Core (Pd+Ni)

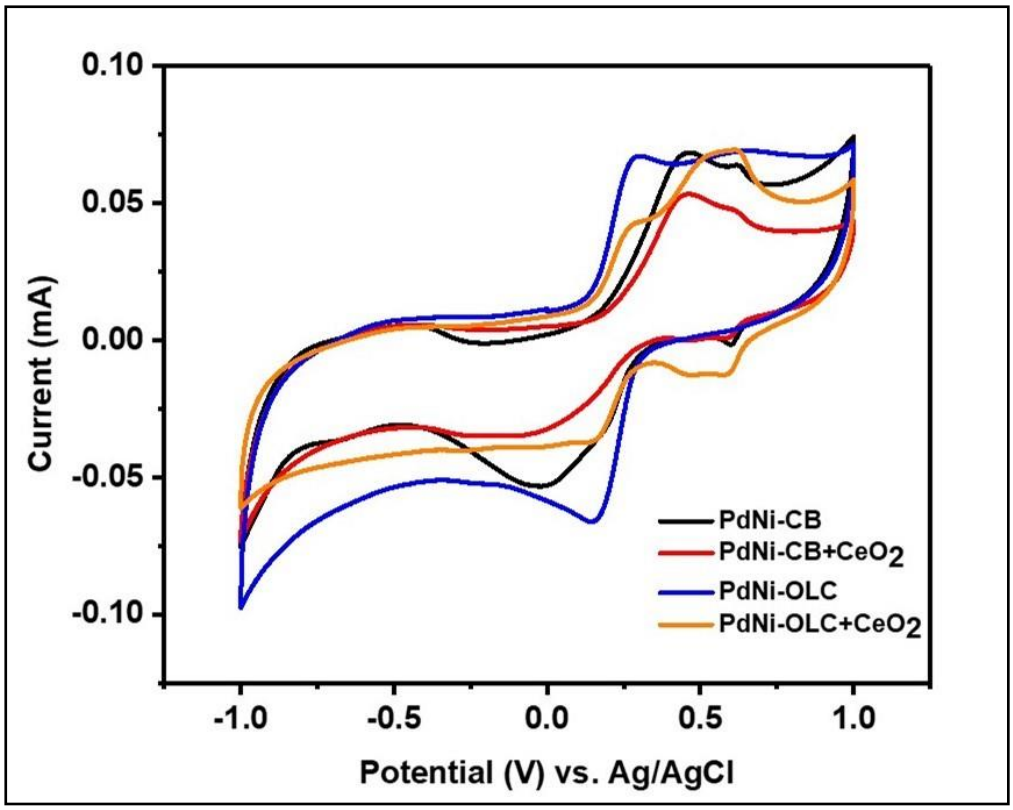

Figure 26: The CV for potassium ferrocyanide/potassium ferricyanide with scan rate of 50 mV/s of the Various PdNi Catalysts

The electrochemical activity of the as-prepared catalyst initially tested in potassium ferrocyanide solution and the results are shown in Figure 26. The CV curves of PdNi-CB, PdNi-CB+CeO_2, and PdNi-OLC+CeO_2 shows the broad peak of oxidation, a small peak at top of the oxidation peak confirming the multielectron oxidation reaction occurred and the cathodic scan

shows the single reduction peak in Figure 26. However, the sharp oxidation and reduction peak is appeared for the PdNi-OLC in Figure 26, indicating the one-electron transfer process and higher current suggest the faster electron transfer through the OLC support. It may suggest that the PdNi-OLC faster kinetics for the ethanol oxidation reaction.

6.2.2. Cyclic Voltammetry (CV) – [KOH+EtOH]

6.2.2.1. Monometallic Core (Pd)

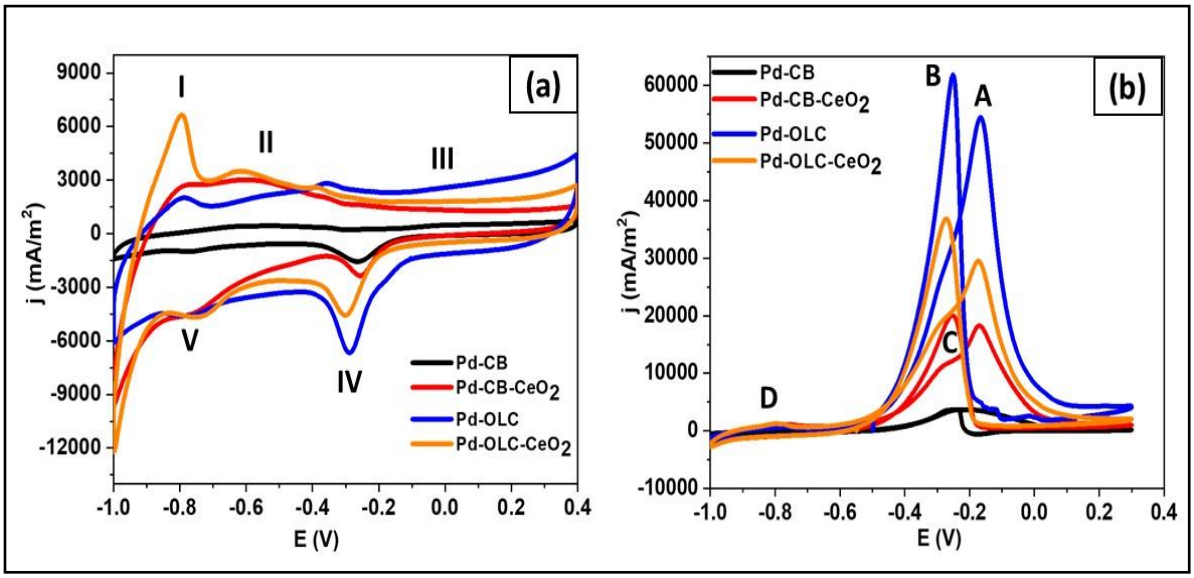

Figure 27: The cyclic voltammogram of the various electrode in (a) 1.0 M KOH (b) 1.0 M KOH + 1.0 M ethanol

Figures 27a and 27b show the cyclic voltagramm (CV) curves of the Pd supported on the various carbon support in 1.0 M KOH with and without 1.0 M ethanol electrolyte, respectively. Generally, the Pd surfaceis considered tobeanactive site for electrochemical redoxreactions. Three potential peaks were observed in Figure 27a. Peak I in the potential range of -0.9 to -0.7 may attribute to the adsorption of hydrogen on the Pd surface. Among Pd-CB, Pd-CB+CeO_2, Pd-OLC, and Pd-OLC-CeO_2, the peak-I current of Pd-OLC+CeO_2 are higher, and it indicates that the hydrogen adsorption occurs only on the Pd surface. Pd-OLC also shows the sharp peak, but the peak for the Pd-CB and Pd-CB+CeO_2 is the broad peak, it may suggest that the CB also helps to the hydrogen adsorption. Further, during the cathodic scan, the hydrogen desorption peak -V was observed at potential -0.7V to -0.8V [6]. The current density for the hydrogen

desorption peak of all the material is almost the same, it indicates that the hydrogen desorption occurs a similar way for all the as-prepared materials.

Peak – II and III in Figure 27a correspond to the adsorption of OH^- and formation of the oxide layer on the catalyst surface, respectively. The Pd-OLC and Pd-OLC+CeO_2 show the better electrochemical double layer formation among all the as-prepared material. Peak – III shows the higher current density compared to the Pd-OLC+CeO_2; it indicates that oxide layer formation was more prone to the Pd surface of the Pd-OLC catalyst. It may contribute that the OH- was adsorbed on the Pd surface of the Pd-OLC catalyst and OH^- may be adsorbed on carbon or CeO_2 of Pd-OLC+CeO_2 catalyst. The reduction of Pd (II) oxide during cathodic sweep confirms byan increase in current density of peak – IV of Pd-OLC is higher than the Pd-OLC+CeO_2. These results may conclude that the Pd-OLC+CeO_2 shows the superior electrochemical performance due to catalyst support provides a platform for the OH^- adsorption restrict the formation of the oxide layer on the catalyst surface [7, 8, 9].

Two main peaks A and B have shown in Figure 27b, which attribute to the positive and negative peak related to the ethanol oxidation activity of the electrocatalyst. The peak – D in Figure 27b corresponds to the hydrogen adsorption and desorption, and the current density intensity was suppressed compared to the peak intensity in 1.0 M KOH. It attributes to the as-prepared catalyst shows the ethanol oxidation reaction. The positive oxidation peak-A attributed to the direct oxidation of ethanol and the peak – B attributed to the intermediate product of ethanol oxidation and/or incompletely oxidized carbonaceous material produced in the system [10, 11].

The higher current density of the Pd-OLC among the all other as-prepared catalyst indicates the superior catalyst activity towards the ethanol oxidation. The current density of the peak – A and B has been decreased for the Pd-OLC+CeO_2. It may associate that the electron transfer from catalyst to the support has been hindered due to the non-conducting behaviour of CeO_2 and lower surface area of the Pd-OLC+CeO_2. The Pd-CB shows the least ethanol oxidation performance may be due to the least surface area. Further, CeO_2 has been added with the carbon support, the other peak – C has been observed, it may attribute to the oxidation of CeO2.

The CV of as-prepared catalysts in 1.0 M KOH and 1.0 M KOH +EtOH confirms that the Pd-OLC shows the superior activity due to the synergistic effect of metal with carbon supportsfor the ethanol oxidation reaction.

Further, the effective catalyticsurface area (ECSA) by using the integral area of the hydrogen adsorption from CV plots the equation below.

$$ECSA = \frac{Q}{S.L}$$

Where, Q = Integral of hydrogen adsorption from CV plot,

S = Charge density constant for Pd (0.424 mC/cm^2), and

L = mass loading of Pd on electrode.

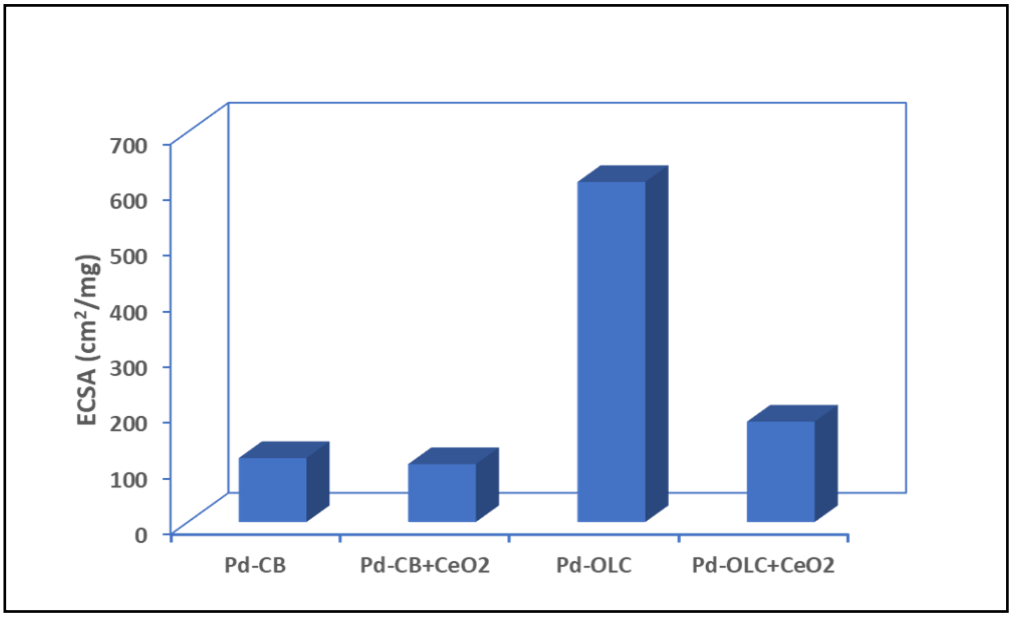

Figure 28: Comparison of effective catalytic surface area for the Various Pd Catalysts

The ECSA values of each electrocatalyst were compared in Figure 28. Among the as-prepared various electrocatalyst, Pd-OLC shows better electrochemical activity with higher ECSA towards the ethanol oxidation. The support OLC helps to faster electron transfer during the electrochemical oxidation.

6.2.2.2. Bimetallic Core (Pd+Ni)

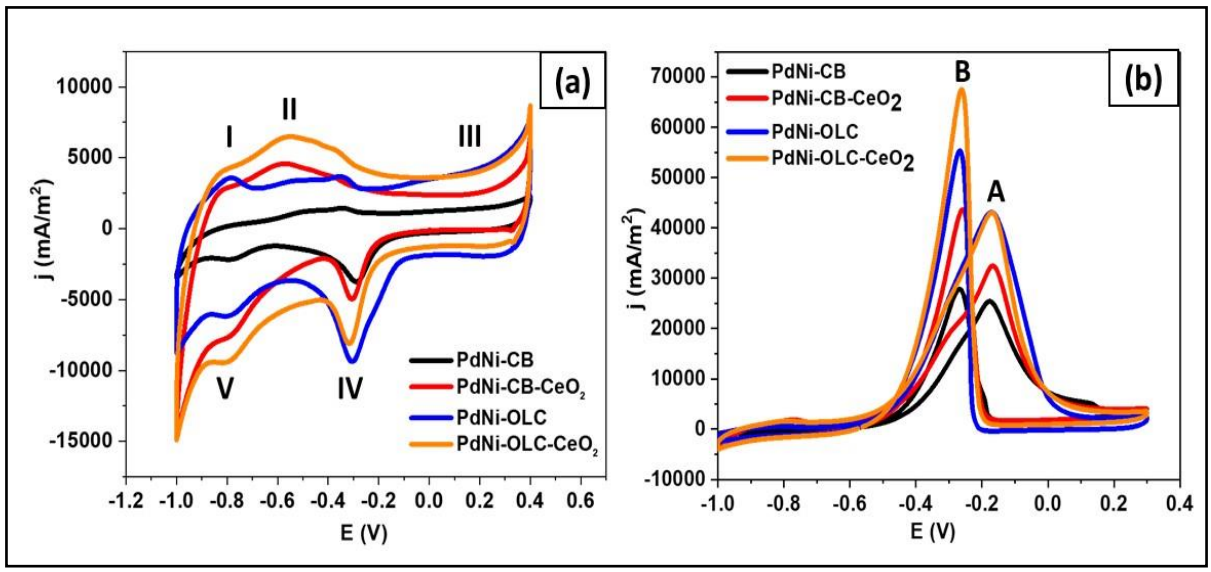

Figure 29: The cyclic voltammogram of the various electrode in (a) 1.0 M KOH (b) 1.0 M KOH + 1.0 M ethanol

Further, we have investigated the catalytic activity of the as-prepared PdNi-CB, PdNi-CB+CeO_2, PDNi-OLC, and the PdNi-OLC+CeO_2 towards the ethanol oxidation reaction by using the cyclic voltagramm (CV) in 1.0 M KOH and 1.0 M KOH +1.0 M EtOH. In Figure 29a, peak – I and V represents the hydrogen adsorption and desorption peak respectively, the current density of the peak – I and V has been increasing from PdNi-CB, PdNi-CB+CeO_2, PdNi-OLC, and to PdNi-OLC+CeO_2. Further peak – IV also present for all the as-prepared catalyst, it suggests that the adsorption of OH^- or formation of an oxide layer on the catalyst surface and peak – V corresponds to the reduction of oxide or desorption of OH^- ion from the catalyst surface [18].

Generally, the mechanism of EOR on Pd can be ascribed as following equations [9, 19, 20].

$$Pd + CH_3CH_2OH \leftrightarrow CH_3CH_2OH \quad [1]$$

$$Pd - (CH_3CH_2OH)_{ads} + 3OH^- \rightarrow Pd - (CH_3CO)_{ads} + 3H_2O + 3e^- \quad [2]$$

$$Pd - (CH_3CO)_{ads} + Pd - OH_{ads} \xrightarrow{r.d.s} Pd - CH_3COOH + Pd \quad [3]$$

$$Pd - CH_3COOH + OH^- \rightarrow Pd + CH_3COO^- + H_2O \quad [4]$$

Equation (1) and (2) have essentially occurred on the Pd surface, however, the generated hydroxyl radical (OH^-) blocks the Pd active surface as shown in equation (3), hence, the ethanol oxidation activity of monometallic Pd may decrease.

Ni is an active metal for the adsorption of OH^-, as shown in equation (3) adsorption of the CH_3CO and OH^- is the determine the ethanol oxidation activity. Therefore, Ni could be involved for the OH^- adsorption and can convert it into $Ni(OH)_2$ and Pd surface sites are used for the ethanol oxidation reaction. Henceforth, Ni can provide a site for the OH^- adsorption and therefore, Pd facilitate the ethanol oxidation at lower onset potential [21]. Therefore, it is expected that the similar behaviour of all the catalyst, but in Figure 29b the current density of each catalyst is different since the carbon support is varied. It suggests that carbon support plays an important role in electron transfer from the catalyst surface. In Figure 29b, the current density of the peak – A is not much increase from PdNi-CB, PdNi-CB+CeO_2, PDNi-OLC, and PdNi-OLC+CeO_2 since it indicates the direct oxidation of ethanol. Whereas, peak – B assigned to the removal of the carbonaceous species and the regeneration of Pd active for the fresh ethanol oxidation reaction.

Figure 29b shows the monotonical increment of the current density of the peak – B as the catalyst support is varied. Although the current density of peak – B of the Pd-OLC+CeO_2 is better than the Pd-OLC the current density of peak – A is similar for both the catalyst. It may attribute that, the generation of the carbonaceous product is higher for Pd-OLC+CeO_2 and incomplete ethanol oxidation. It indicates that the carbon support plays an important role along with catalyst surface for the ethanol oxidation.

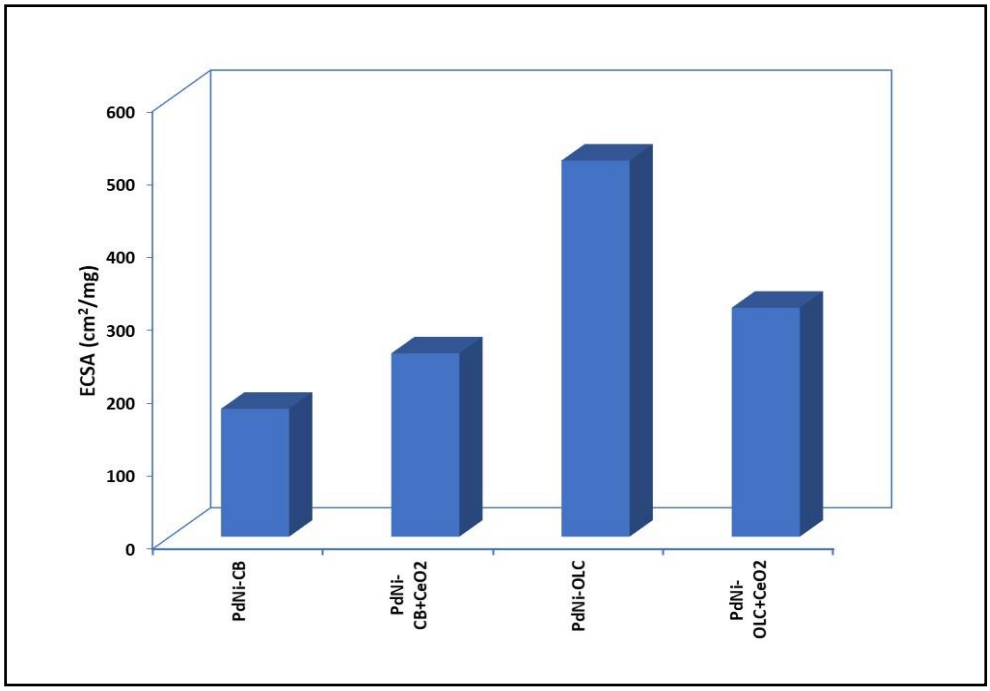

Figure 30: Comparison of effective catalytic surface area for the Various PdNi Catalysts

From Figure 30, it observed that the ECSA of the PdNi-OLC is 515.8 cm^2/mg and the second highest among of all the as-prepared catalyst. It shows that Pd-OLC (and PdNi-OLC) possess a high surface area for the electrochemical performance and current density of the anodic peak of the direct-ethanol oxidation for the Pd-OLC and Pd-OLC+CeO_2. This finding indicates that the OLC promotes the ethanol oxidation reaction by allowing a higher electrochemically active area.

6.2.3. Linear Sweep Voltammetry (LSV) and Tafel Plots

6.2.3.1. Monometallic Core (Pd)

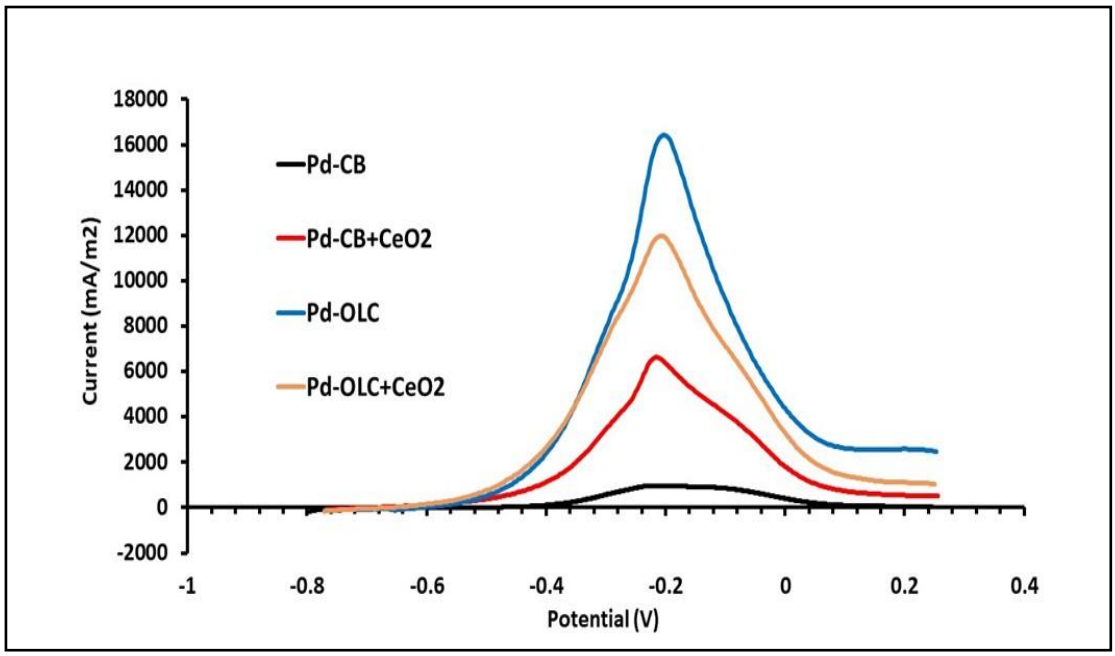

Figure 31: A quasi-steady-state curve of the ethanol oxidation on the Various Pd Catalysts in 1.0M KOH + 1.0 M

To further study the EOR, a typical liner sweep voltagramm at the sweep rate of 1 mV/s has been carried out on as-prepared electrocatalyst in 1.0 M KOH + 1.0 M EtOH, and the result shown in Figure 31.

The current density at potential – 0.2 V is gradually increasing from Pd-CB, Pd-CB+CeO_2, Pd-OLC+CeO_2, and Pd-OLC in Figure 31. It may attribute to the electron transfer from catalyst surface to support is faster. Therefore Pd-OLC shows the superior performance among all the as-prepared electrocatalyst. The Pd-OLC and Pd-OLC+CeO_2 show the approximately same onset potential compared to the Pd-CB and Pd-CB+CeO_2. However, the current density of the Pd-OLC is much higher than that of Pd-OLC+CeO_2, it indicates that the Pd-OLC possess the highest ethanol oxidation kinetics. It confirms that the carbon support is helpful to enhance the kinetics and lower the overpotential for the EOR. The high surface area of the Pd-OLC and graphitized carbon is responsible for the superior EOR.

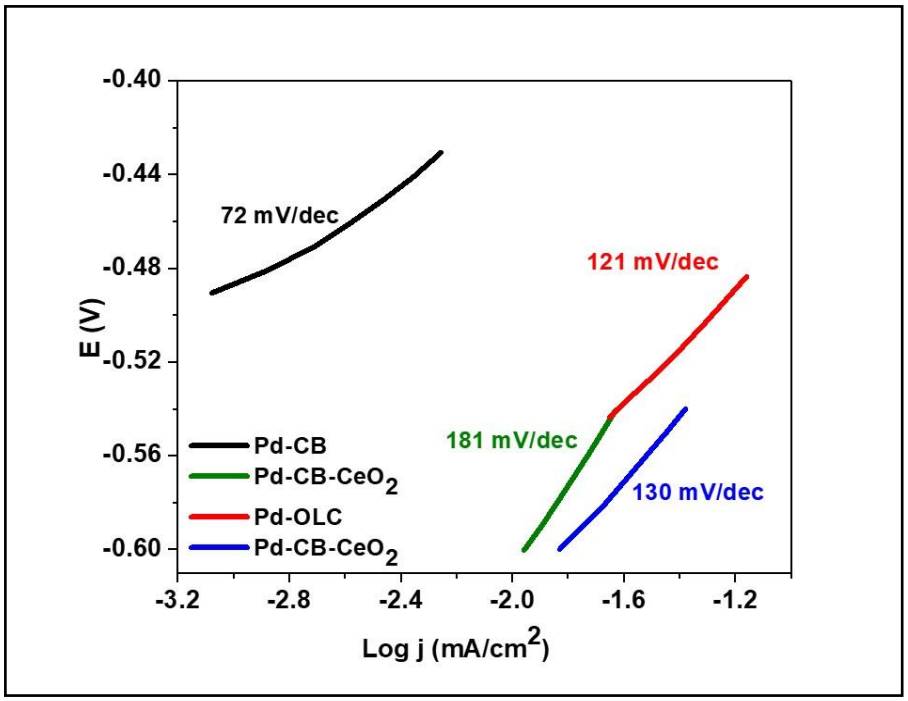

Figure 32: Tafel Plots in 1.0 M KOH + 1.0 M Ethanol with sweep rate of 1mV/s on Various PdNi Catalysts

In addition, the compared Tafel plots of ethanol oxidation were obtained in 1.0 M KOH+1.0 M EtOH and the values of each catalyst are shown in Figure 32. The lowest value Pd-OLC was observed among all the as-prepared catalyst, it indicates the ethanol oxidation is more favourable on the Pd-OLC. Tafel slope values of Pd-OLC 121 mV/dec which is very close to the ethanol electrooxidation controlled by the adsorption of OH^- value is 120 mV/dec [12, 13].

Note: It is expected that Pd-OLC would posses the lowest (or atleast a relatively low) slope compared to the others. However, after multiple iterations, these results have not changed.

4.2.3.2. Bimetallic Core (Pd+Ni)

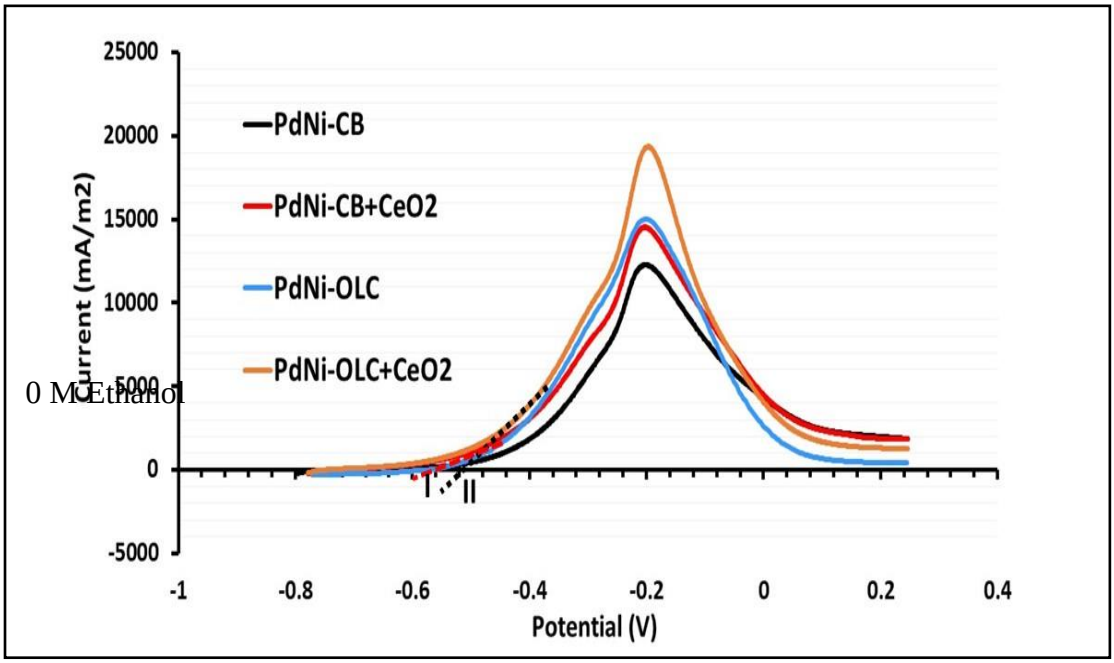

Figure 33: A quasi-steady-state curve of the ethanol oxidation on the Various PdNi electrodes in 1.0M KOH + 1.0 M Ethanol

The linear sweep voltammetry (LSV) curve of the various catalyst has been tested and the results are shown in Figure 33. The as-prepared catalyst shows the very little increment in current density from the PdNi-OLC and the PdNi-OLC+CeO_2, but the onset potential is found to be -0.62 and -0.58 V, respectively and shown by I and II in Figure 33. The lowest onset potential of PdNi-OLC suggests that the superior electrochemical performance among all the as-prepared catalyst.

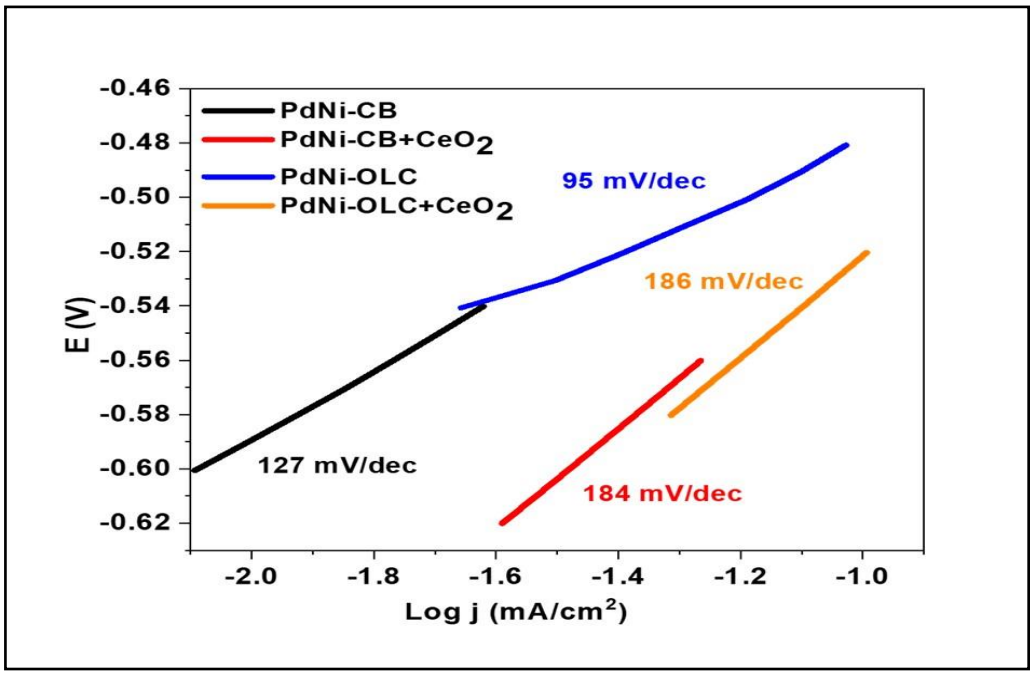

Figure 34: Tafel Plots in 1.0 M KOH + 1.0 M Ethanol with sweep rate of 1mV/s on Various PdNi Catalysts

To further understand the electrochemical performance of as-prepared catalyst Tafel slop has been shown in Figure 34. The lowest Tafel slope value of 95 mV/dec was obtained by the PdNi-OLC catalyst and the other values are shown in Figure 34. It confirms that PdNi-OLC is the best catalyst among all the as-prepared catalyst.

Although all catalyst possesses the bimetallic PdNi alloy, but the support is varied and hence the ethanol oxidation activity of the catalyst is varied. PdNi-OLC shows the best catalytic activity towards the ethanol oxidation because of the high surface area and graphitic nature of the OLC.

The Tafel value is close to the 120 mV/dec, it suggests that the ethanol oxidation was controlled by the OH^- adsorption mechanism. The as-prepared PdNi-CB, PdNi-CB+CeO_2, and PdNi-OLC+CeO_2 show the 127, 184 and 186 mV/dec values, respectively. It suggests that the PdNi-CB is also controlled by the OH^- adsorption mechanism. The CeO_2 added to support does not follow the OH^- adsorption mechanism.

6.2.4. Electrochemical Impedance Spectroscopy (EIS)

6.2.4.1. Monometallic Core (Pd)

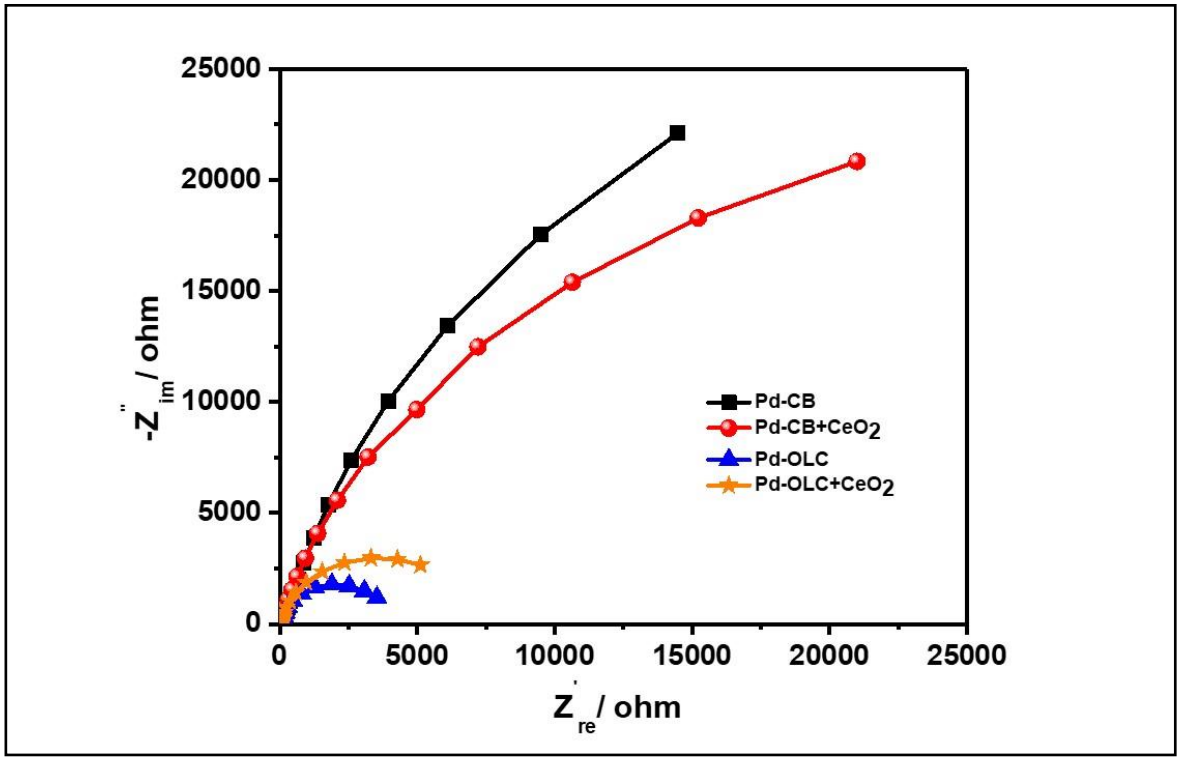

Figure 35: Nyquist plot of Various Pd Catalysts

Further to understand the charge transfer resistance for prepared catalyst the Nyquist plots are made and shown in Figure 35. The charge transfer resistance (R_{ct}) provides a resistance between the surface of the electrode and the electrolyte when the ethanol oxidized at the surface of electrocatalysts. The lower the R_{ct} signifies the faster the charge transfer and hence lower the obstacle for electron transfer from electrocatalyst surface. Hence, the lower the R_{ct} value of the Pd-OLC indicates that the better the electrocatalytic performance of the catalyst. Figure 35 shows the lower R_{ct} of the Pd-OLC among all the other catalyst and impedance results are consistent with CV, LSV, and Tafel plots. Therefore, it can be concluded that the carbon support is important to enhance the performance of the ethanol electrooxidation [14].

6.2.4.2. Bimetallic Core (Pd+Ni)

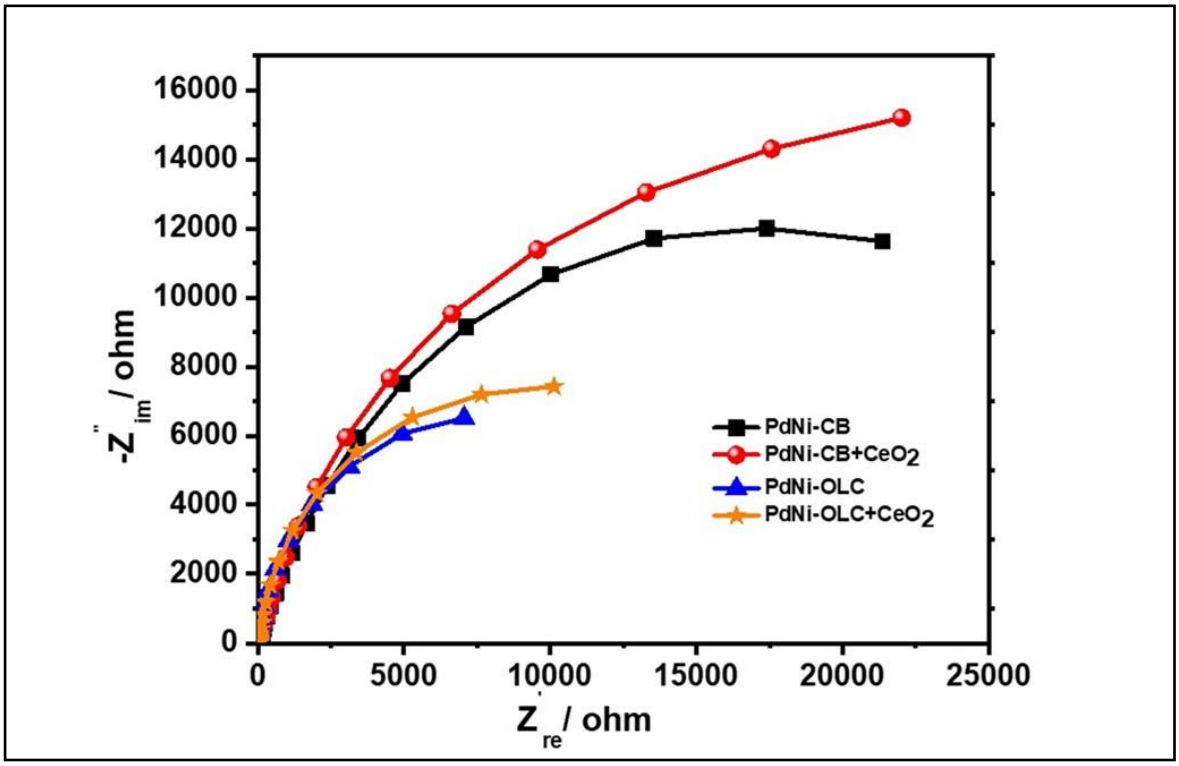

Figure 36: Nyquist plot of Various PdNi Catalysts

To understand the charge transfer between the electrode-electrolyte surface, the electrochemical impedance spectroscopy (EIS) was studied and the result is shown in Figure 30. In the case of EIS, semicircle in Figure 36 shows the charge transfer (R_{ct}) and lower the R_{ct}faster the charge transfer and lesser the obstacle for electron transfer from the catalyst surface to support. Figure 36 shows the lower R_{ct} of the Pd-OLC among all the other catalyst and impedance results are consistent with CV, LSV, and Tafel plots. Therefore, it can be concluded that the carbon support is important to enhance the performance of the ethanol electrooxidation and OLC serves as a superior medium to the standard Carbon Black. The Values can be seen in the table below.

Table 4: EIS data for ALL Catalysts

	EIS Constants				Deviations				
Catalyst	Rs (Ohm)	CPE (F.s^[a-1])	Rct (Ohm)	a2	Rs	CPE	Rct	a2	Pseudo C equivalent
Pd/CB	64,82	4,84E-05	76 216	0,8508	0,1938	1,33E-08	6 614	0,5002	6,09E-05
PdNi/CB	43,15	3,01E-05	33 852	0,7898	0,2016	6,76E-09	7,612	0,5	3,03E-05
Pd/CB+CeO2	3,909	3,58E-05	59 899	0,8085	0,1976	8,49E-09	17,81	0,5001	4,28E-05
PdNi/CB+CeO2	17,55	3,17E-05	41 950	0,7828	0,2012	7,27E-09	10,85	0,5	3,44E-05
Pd/OLC	58,29	1,40E-04	3 964	0,9398	0,1934	1,61E-07	3,093	0,5016	1,35E-04
PdNi/OLC	35,25	1,08E-04	14 695	0,9219	0,1906	7,79E-08	7,082	0,5009	1,13E-04
Pd/OLC+CeO2	29,47	1,18E-04	7 189	0,8799	0,1952	1,09E-07	5,235	0,5002	1,15E-04
PdNi/OLC+CeO2	30,14	7,16E-05	17 440	0,895	0,1928	3,73E-08	7,301	0,5004	7,34E-05

7. Conclusion

In summary, the monometallic Pd dispersed on the various support such as CB, CB+CeO_2, OLC, and OLC+CeO_2 and tested for the ethanol electrooxidation. Further the study was extend to the disersion of bimetallic PdNi on the various support such as CB, CB+CeO_2, OLC, and OLC+CeO_2 and tested for the ethanol electrooxidation. The presence of graphitized carbon in OLC, the non-graphitized carbon of CB, and presence of Ni atom for bimetallic PdNi has been identified by the XRD spectrum. The broad peak of Pd in XRD confirm the insertion of Ni into the crystal lattice of Pd. The amount of loading and surface area of the various catalyst has been characterized by the TGA and N2 adsorption-desorption isotherm, respectively.The Pd-OLC and PdNi-OLC possess the highest surface area of 357.73 and 373.53 m2/g respectively among all other various support has been observed through the Nitrogen adsorption-desorption isotherm technique. The as-prepared Pd-OLC and PdNi-OLC shows the highest ECSA among all the as-prepared catalyst. The lowest onset potential and the highest current density of the Pd-OLC and PdNi-OLC indicates the highest ethanol electrooxidation kinetics than as-prepared electrocatalyst. The lowest Tafel slope value of 86 and 121 mV/dec for PdNi-OLC and Pd-OLC, respectively suggest the ethanol electrooxidation through the OH- adsorption mechanism. The lower Rct value of the PdNi-OLC and Pd-OLC indicates the better electrocatalytic performance of the catalyst. The superior electrochemical performance of the Pd-OLC and PdNi-OLC could occur due to the graphitized and high surface area of OLC among other supports.

8. The Way Forward

The results produced from this research clearly indicate the potential OLC has in this field. With it's incredible conductivity, surface area, and overall performance boost to it's carbon black counterpart, more research and effort should be placed on phasing out less impactful supports and allowing OLC to become the norm.

Due to time, money, and accessibility limitations, a more extensive research study was not possible for this project. However, techniques such as TEM, XPS, and ICP-OES should further used to get a more detailed understanding of the material structure. The catalysts were also only tested as a 3 electrode system which serves well for the purposes of this project but a fully functioning MEA would prove to be a better system to test these materials and should be considered in the near future. As this would allow us to rate the:

- Sensitivity: to determine it's detection limits and how impactful variations in ethanol gas concentratios effect the system output.
- Selectivity: should be tested to validate that the AGFCS is highly responsive to Ethanol but not other alcohols / gases
- Consistency: Output should be consistent with at least a 95% confidence band.
- Reliability: The system should work under various conditions and last a significant amount of time

This research was done for the purposes of gaining knowledge and I would hope that it contributes to the fight against driving under the influence.

Thank You

References – Results and Discussion

1. Bokobza, L., Bruneel, J. L., and Couzi, M. (2015). “Raman spectra of carbon-based materials (from graphite to carbon black) and of some silicone composites.” C—Journal of Carbon Research, 1(1), 77-94.

2. Ghosh, S., Ganesan, K., Polaki, S. R., Ravindran, T. R., Krishna, N. G., Kamruddin, M., and Tyagi, A. K. (2014). “Evolution and defect analysis of vertical graphene nanosheets.” Journal of Raman Spectroscopy, 45(8), 642-649.

3. Iqbal, M., Li, C., Jiang, B., Hossain, M. S. A., Islam, M. T., Henzie, J.,and Yamauchi, Y. (2017). “Tethering mesoporous Pd nanoparticles to reduced graphene oxide sheets forms highly efficient electrooxidation catalysts.” Journal of Materials Chemistry A, 5 (40), 21249-21256.

4. Zhang, Q., Jiang, L., Wang, H., Liu, J., Zhang, J., Zheng, Y., Li, F., Yao, C., and Hou, S. (2018). “Hollow graphitized carbon nanocage supported Pd catalyst with excellent electrocatalytic activity for ethanol oxidation.” ACS Sustainable Chemistry & Engineering, 6 (6), 7507-7514.

5. Li, Z., Yang, R., Li, B., Yu, M., Li, D., Wang, H., & Li, Q. (2017). “Controllable synthesis of graphene/NiCo2O4 three-dimensional mesoporous electrocatalysts for efficient methanol oxidation reaction.” Electrochimica Acta, 252, 180-191.

6. Vračar, L. J., Burojević, S., &Krstajić, N. (1998). “The surface processes at Pd–Ni alloy in acid and alkaline solutions.” International journal of hydrogen energy, 23 (12), 1157-1164.

7. Takamura, T.; Minamiyama, K. I. (1965). “Anodic oxidation of methanol at palladium electrode in alkaline solution.” Journal of The Electrochemical Society, 112 (3), 333-335.

8. Prabhuram, J., Manoharan, R., &Vasan, H. N. (1998). “Effects of incorporation of Cu and Ag in Pd on electrochemical oxidation of methanol in alkaline solution.” Journal of applied electrochemistry, 28 (9), 935-941.

9. Liang, Z. X., Zhao, T. S., Xu, J. B., and Zhu, L. D. (2009). “Mechanism study of the ethanol oxidation reaction on palladium in alkaline media.” Electrochimica Acta, 54 (8), 2203-2208.

10. Sahin, O., &Kivrak, H. (2013). “A comparative study of electrochemical methods on Pt–Ru DMFC anode catalysts: the effect of Ru addition.” International journal of hydrogen energy, 38 (2), 901-909.

11. Li, Z., Zhang, L., Yang, C., Chen, J., Wang, Z., Bao, L., Wu, F., and Shen, P. (2019). “Graphitized carbon nanocages/palladium nanoparticles: Sustainable preparation and electrocatalytic performances towards ethanol oxidation reaction.” International Journal of Hydrogen Energy, 44 (12), 6172-6181.

12. Jiang, L., Hsu, A., Chu, D., and Chen, R. (2010). “Ethanol electro-oxidation on Pt/C and PtSn/C catalysts in alkaline and acid solutions.” International Journal of Hydrogen Energy, 35 (1), 365-372.

13. Shen, S. Y., Zhao, T. S., & Xu, J. B. (2010). “Carbon supported PtRh catalysts for ethanol oxidation in alkaline direct ethanol fuel cell.” international journal of hydrogen energy, 35 (23), 12911-12917.

14. Yang, Y., Yu, S., Gao, L., Wang, X., and Yan, S. (2019). “The Properties of PdRu/C with respect to the Electro-oxidation of Methanol and Ethanol.” INTERNATIONAL JOURNAL OF ELECTROCHEMICAL SCIENCE, 14 (1), 1270-1282.

15. Kowal, A., Li, M., Shao, M., Sasaki, K., Vukmirovic, M. B., Zhang, J., Marinkovic, N.S., Liu, P., Frenkel A. I., and Adzic, R. R. (2009). “Ternary Pt/Rh/SnO 2 electrocatalysts for oxidizing ethanol to CO2”. Nature materials, 8 (4), 325-330.

16. Sulaiman, J. E., Zhu, S., Xing, Z., Chang, Q., & Shao, M. (2017). “Pt–Ni octahedra as electrocatalysts for the ethanol electro-oxidation reaction.” ACS Catalysis, 7 (8), 5134-5141.

17. Yang, H., Coutanceau, C., Léger, J. M., & Alonso-Vante, N. (2005). “Methanol tolerant oxygen reduction on carbon-supported Pt–Ni alloy nanoparticles.” Journal of Electroanalytical Chemistry, 576 (2), 305-313.

18. Na, H., Zhang, L., Qiu, H., Wu, T., Chen, M., Yang, N., Li, L., Xing, F., and Gao, J. (2015). ‘A two step method to synthesize palladium–copper nanoparticles on reduced graphene oxide and their extremely high electrocatalytic activity for the electrooxidation of methanol and ethanol.” Journal of Power Sources, 288, 160-167.

19. Tripković, A. V., Popović, K. D., and Lović, J. D. (2001). “The influence of the oxygen-containing species on the electrooxidation of the C1–C4 alcohols at some platinum single crystal surfaces in alkaline solution.” *Electrochimica Acta*, **46** (20-21), 3163-3173.

20. Liu, J., Ye, J., Xu, C., & Tong, Y. (2007). "Kinetics of ethanol electrooxidation at Pd electrodeposited on Ti." *Electrochemistry Communications*, **9** (9), 2334-2339.

21. Zhang, Z., Xin, L., Sun, K., and Li, W. (2011). "Pd–Ni electrocatalysts for efficient ethanol oxidation reaction in alkaline electrolyte." *International Journal of Hydrogen Energy*, **36** (20), 12686-12697.

University of the Witwatersrand, Johannesburg, South Africa

Faculty of Engineering and the Built Environment

School of Chemical and Metallurgical Engineering

Plagiarism Declaration for Postgraduate Research Submission

I, Suhail Ahmed Musa (Student number: 742699), am a student registered for Masters in Chemical Engineering in the year 2018. I hereby declare the following:

- I am aware that plagiarism (the use of someone else's work without their permission and/or without acknowledging the original source) is wrong.
- I confirm that the work submitted for assessment for the above course is my own unaided work except where I have explicitly indicated otherwise.
- I have followed the required conventions in referencing the thoughts and ideas of others.
- I understand that the University of the Witwatersrand may take disciplinary action against me if there is a belief that this is not my own unaided work or that I have failed to acknowledge the source of the ideas or words in my writing.

Student Signature:  Date: 03/04/2020